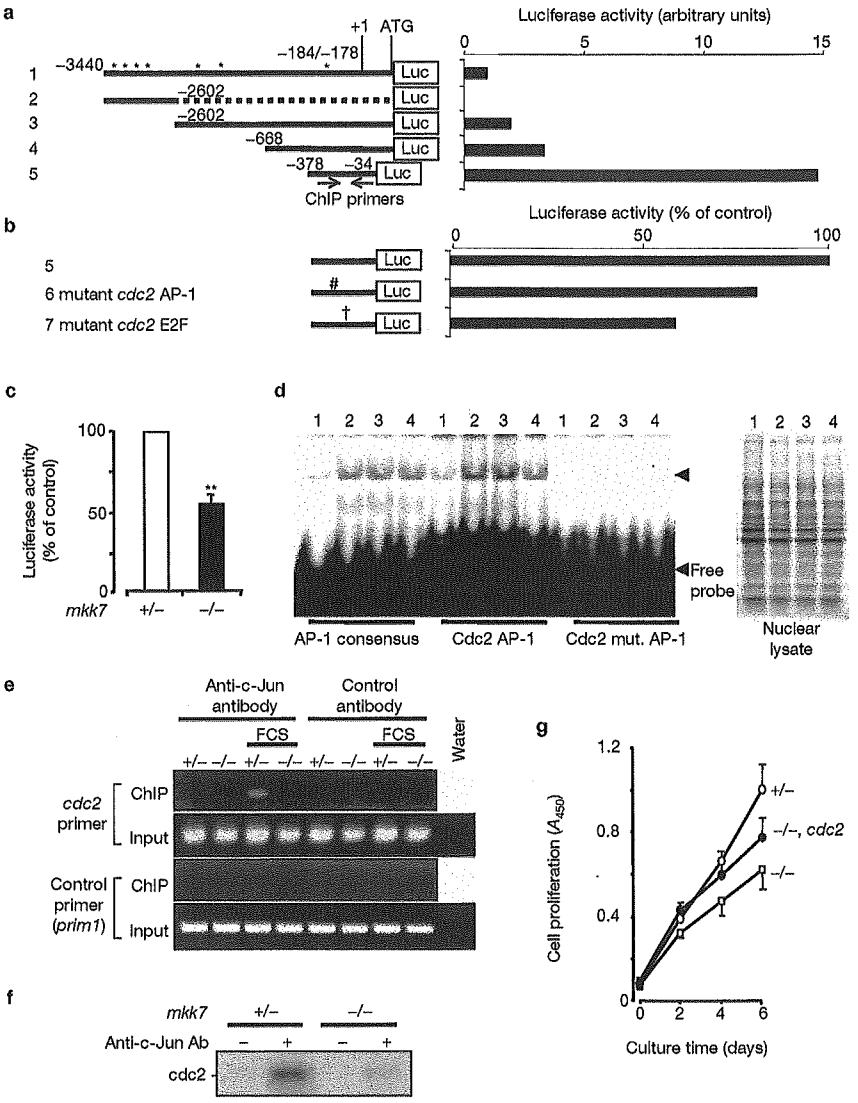

Figure 5 MKK7 controls *cdc2* promoter activity. (**a**, **b**) MKK7 enhances *cdc2* promoter activity in luciferase reporter assays. The indicated constructs were transfected into phoenix E cells and luciferase activities were measured. Potential AP-1-binding sites based on *in silico* analysis are indicated with an asterisk. E2F and *cdc2* AP-1 mutations are indicated as # and †, respectively. Mean values of three experiments are shown. (**c**) Luciferase reporter assays in *mkk7*$^{+/-}$ *and mkk7*$^{-/-}$ MEFs (passage 4). Construct 5 in **a** was used to determine *cdc2* promoter activity. One representative experiment is shown. $^{**}P < 0.01$ between *mkk7*$^{+/-}$ and *mkk7*$^{-/-}$ MEFs. (**d**) Cell extracts were obtained from wild-type MEFs, and EMSAs were performed using consensus AP-1, wild-type *cdc2* AP-1, and mutant *cdc2* AP-1 oligonucleotides. Lane 1, 0.5% serum-starved cells; lane 2, exponentially proliferating cells; lane 3, 20% serum stimulation (30 min); lane 4, 10 J m^{-2} UV stimulation. The right panel shows the amounts of nuclear lysates as loading controls. (**e**, **f**) ChIP assay of c-Jun bound to the *cdc2* AP-1 site in *mkk7*$^{+/-}$and *mkk7*$^{-/-}$ MEFs (passage 4). The positions of the ChIP primers are shown in **a**. The primers for *prim1* gene, which is located on the same chromosome as *cdc2* and does not contain AP-1 consensus sequences in its promoter locus, were used as control. Input indicates total cell lysates before immunoprecipitation to ensure equal loading. ChIP PCR products were visualized using ethidium bromide staining (**e**) or α-^{32}P-dCTP incorporation (**f**). (**g**) Ectopic expression of wild-type CDC2 partially restores the decreased proliferation of passage-4 *mkk7*$^{-/-}$ MEFs. Mean proliferation values of three experiments are shown.

reduced proliferation of *mkk7*$^{-/-}$ MEFs is not the result of increased cell death.

To determine the role of MKK7 in cell proliferation, MEFs were cultured for over 150 days. Similarly to our proliferation data, *mkk7*$^{-/-}$ MEFs did not show any significant differences in population doubling within the first three passages (Fig. 3a). However, during subsequent passages, loss of MKK7 resulted in a marked decrease in cell numbers (Fig. 3a). In all MEF cell lines (five independent cultures) analysed, loss

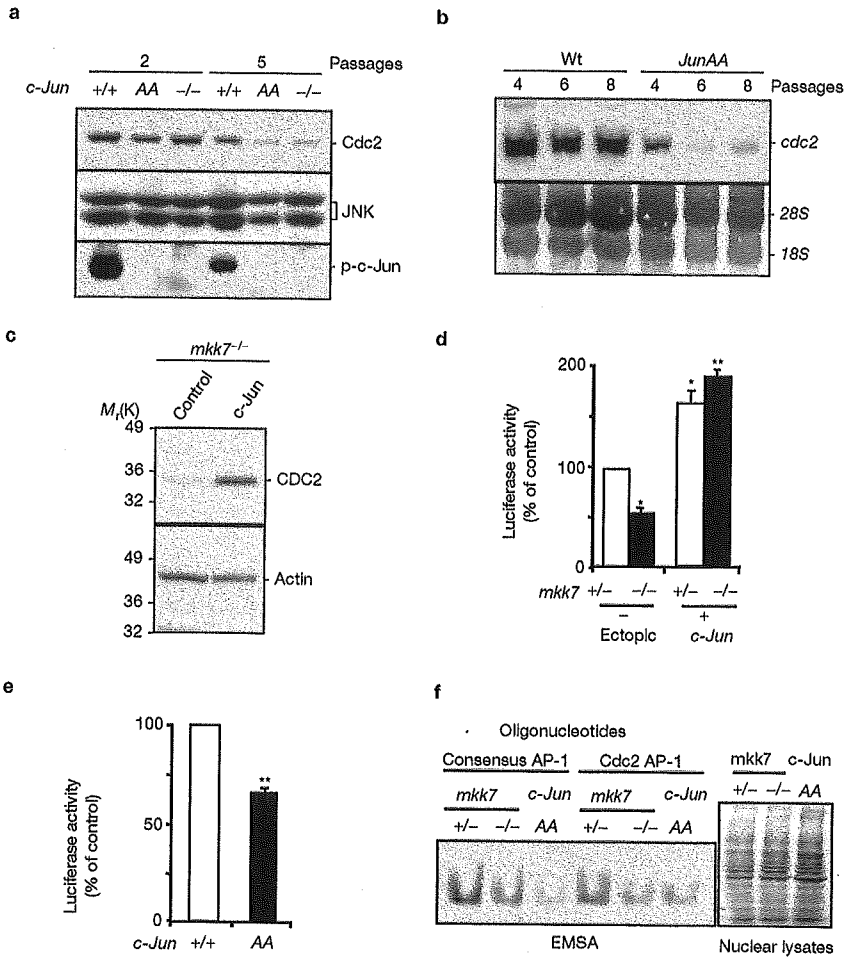

Figure 6 c-Jun regulates CDC2 expression. **(a)** Expression levels of CDC2 protein, JNK and phospho-c-Jun in passage-2 and -5 *c-jun*$^{-/-}$ and *c-junAA* MEFs. **(b)** Expression levels of *cdc2* mRNA in passage-4, -6 and -8 wild-type and *c-junAA* MEFs. Total RNA, stained with methylene blue, is also shown (bottom). **(c)** Overexpression of c-Jun upregulates CDC2. pBabe (control) or pBabe-c-Jun were introduced into *mkk7*$^{-/-}$ MEFs and CDC2 protein expression was determined by western blotting. For the whole blots of **a–c**, see Supplementary Information Fig. S4c–e. **(d)** Luciferase reporter assays in *mkk7*$^{+/-}$ *and mkk7*$^{-/-}$ MEFs in the presence and absence of overexpressed c-Jun (passage 4). pBabe-c-Jun or pBabe were introduced in MEFs and construct 5 from Fig. 5a was used to determine *cdc2* promoter activity. $*P < 0.05$, $**P < 0.01$ versus *mkk7*$^{+/-}$ MEFs transfected with control pBabe. **(e)** Luciferase reporter assays of *cdc2* promoter activity in c-*junAA* MEFs. $**P < 0.01$ between *c-JunAA* and wild-type control MEFs. **(f)** EMSA assay in *mkk7*$^{+/-}$, *mkk7*$^{-/-}$ and *c-JunAA* MEF cell extracts using consensus AP-1 and *cdc2* AP-1. The right panel shows loading of nuclear lysates.

of MKK7 resulted in extended crisis and premature senescence, as determined by senescence-associated β-galactosidase (SA-β-gal) staining (Fig. 3b and top panel in Fig. 3c) and an enlarged and flattened cell morphology (Fig. 3c, bottom), both of which are established features of senescence in MEFs[18]. Ectopic expression of wild-type MKK7, but not kinase-dead MKK7, rescued premature senescence in *mkk7*$^{-/-}$ MEFs (Fig. 3b, c, and data not shown). Overexpression of MKK7 also increased proliferation and delayed the onset of crisis and senescence in wild-type MEFs (data not shown). Moreover, genetic inactivation of MKK4 in MEFs resulted in reduced proliferation doubling times and premature senescence, indicating that both MKK4 and MKK7 are essential for these cellular processes (data not shown). These results are consistent with previous data showing that loss of JNK1/JNK2 in MEFs results in reduced proliferation[17] and that inactivation of c-Jun in MEFs results in premature senescence and impaired proliferation[19]. Thus, the MKK4–MKK7-regulated JNK signalling pathway is directly responsible for the control of proliferation and cellular senescence.

Defective G2/M cell-cycle progression

As *mkk7*$^{-/-}$ MEFs undergo premature senescence and display reduced proliferation, we analysed the cell-cycle profiles in *mkk7*$^{-/-}$ MEFs after five passages. Surprisingly, whereas senescent cells are normally arrested at the G1 phase[20], *mkk7*$^{-/-}$ MEF lines displayed more G2/M

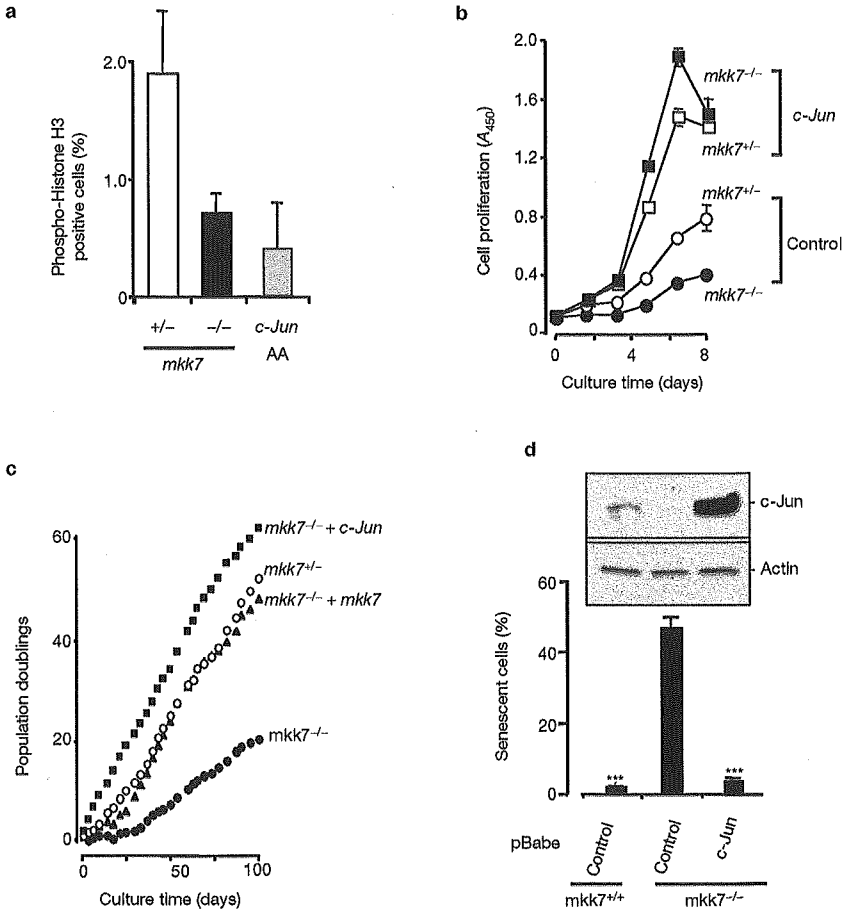

Figure 7 c-Jun rescues senescence and proliferation defects in *mkk7*$^{-/-}$ MEFs. (**a**) Phospho-Histone H3-positive cells in *mkk7*$^{+/-}$, *mkk7*$^{-/-}$ and *c-JunAA* MEFs. Mean values from three independent experiments are shown. (**b**) Cell proliferation (passage 4) was determined at the indicated times. pBabe (control) or pBabe-c-Jun was introduced into *mkk7*$^{+/-}$ and *mkk7*$^{-/-}$ MEFs. (**c**) Growth curves of *mkk7*$^{+/-}$ and *mkk7*$^{-/-}$ MEFs. pBabe (control), pBabe-c-Jun or pBabe-MKK7 were introduced into *mkk7*$^{+/-}$ and *mkk7*$^{-/-}$ MEFs and population doublings were determined as in Fig. 3a. (**d**) c-Jun overexpression rescues cellular senescence of *mkk7*$^{-/-}$ MEFs. Senescence was determined at passage 5 by SA-β-galactosidase staining. Western blots show expression levels of c-Jun and β-actin (for whole blots, see Supplementary Information Fig. S4f). ***$P < 0.001$ versus *mkk7*$^{-/-}$ MEFs.

boundaries when compared with *mkk7*$^{+/-}$ (Fig. 3d) or wild-type (data not shown) MEFs. Re-expression of MKK7 in *mkk7*$^{-/-}$ MEFs abolished the G2/M cell-cycle arrest (Fig. 3d). Synchronized *mkk7*$^{-/-}$ MEFs did not show an apparent defect in G1-to-S-phase entry; however, *mkk7*$^{-/-}$ MEFs displayed an extended G2/M phase after serum stimulation (data not shown). To address whether *mkk7*-deficient MEFs are arrested in G2 or M phase, phospho-Histone H3 staining was performed. Histone H3 is phosphorylated at Ser 10 during M phase, but not at G2 (refs 21, 22). *mkk7*$^{-/-}$ MEFs showed less phospho-Histone H3-positive cells than *mkk7*$^{+/-}$ cells (Fig. 3e), indicating that *mkk7*$^{-/-}$ MEFs are arrested in G2 phase rather than M phase. These data show that loss of MKK7 in MEFs results in an unexpected defect in G2/M cell-cycle progression.

Interestingly, environmental stresses, such as UV irradiation and oxidative stress, trigger a G2/M arrest[23–25] and premature senescence[26]. Therefore, low-passage *mkk7*$^{+/-}$ and *mkk7*$^{-/-}$ MEFs were treated with hydrogen peroxide and UV to test the role of the MKK7–JNK in G2/M arrest and senescence in response to these environmental stresses. *mkk7*$^{-/-}$ MEFs displayed more susceptibility to stress-induced premature senescence (Fig. 3f) and G2/M block (see Supplementary Information, Fig. S2a, b). Thus, MKK7 regulates cellular senescence and G2/M progression in response to environmental stress

Impaired CDC2 expression and CDC2 activity in *mkk7*$^{-/-}$ MEFs

To identify the mechanism through which MKK7 regulates proliferation and G2/M cell cycle progression, we examined the expression levels of molecules known to be involved in cell-cycle control and senescence. Expression of ERK1/2, p38-MAPK, MKK4, JNKs, JunB, JunD, and ATF2 were comparable between *mkk7*$^{+/+}$, *mkk7*$^{+/-}$, and *mkk7*$^{-/-}$ MEFs (Fig. 4a). Consistent with the *in vitro* kinase assays showing reduced JNK activation (Fig 2a), phosphorylation and expression of c-Jun were reduced in *mkk7*$^{-/-}$ MEFs (Fig. 4a). Expression of the cell-cycle molecules cyclin B (Fig. 4a), p16, p21, cyclin D1 (Fig. 4b), p27 and cyclin E (data not shown) were comparable between the different genotypes. Similarly to previously results[15], we did not observe obvious changes in

p53 expression (Fig. 4a). Moreover, telomerase activity in *mkk7*$^{-/-}$ MEFs was comparable with MKK7-expressing MEFs (data not shown).

Intriguingly, a marked reduction in the expression of CDC2 protein was observed (Fig. 4a). CDC2 has been shown to be essential for G2/M cell-cycle progression in multiple organisms[27,28]. Reduced expression of CDC2 in *mkk7*$^{-/-}$ MEFs correlated with the numbers of cell passages; CDC2 expression seemed normal at early passages (passage 1–2: normal G2/M phase, proliferation and population doubling), and consistent with the proliferation defect, it was rapidly downregulated thereafter (passage 4–10: G2/M block and reduced proliferation and population doubling; Fig. 4b). Expression levels of cyclin D1, p21, p16 (Fig. 4b), p53, GADD45 and JNK (data not shown) were similar in *mkk7*$^{+/-}$ and *mkk7*$^{-/-}$ MEFs at the different passage numbers examined. *mkk7*$^{-/-}$ MEFs exhibited reduced JNK activation and delayed CDC2 up-regulation after serum stimulation (data not shown). Reduced expression of *cdc2* mRNA was also observed in *mkk7*$^{-/-}$ MEFs (Fig. 4c). Importantly, cyclin B1-associated CDC2 kinase activity was markedly reduced in *mkk7*$^{-/-}$ MEFs (Fig. 4d), indicating that reduced CDC2 expression correlates with impaired cyclin B1/CDC2 activity. These data suggest that CDC2 is a potential molecular target for MKK7 regulated stress kinase signalling.

Impaired proliferation and CDC2 expression in primary *mkk7*$^{-/-}$ hepatocytes

Whereas hepatogenesis seemed normal at earlier stages of embryogenesis in *mkk7*$^{-/-}$ embryos, mutation of MKK7 results in embryonic lethality that correlated with impaired liver development (Fig. 1). The defective development of the parenchymal liver in *mkk7*$^{-/-}$ embryos seemed to parallel our results in *mkk7*-null MEFs, which display normal proliferation at initial passages that is rapidly followed by a proliferation defect. Therefore, proliferation was analysed in hepatocytes and haematopoietic liver progenitor cells from E11.5 *mkk7*$^{-/-}$ embryos. Haematopoietic precursor cells from both *mkk7*$^{+/-}$ and *mkk7*$^{-/-}$ embryos stained positive for 5-bromo-2′-deoxyuridine (BrdU) labelling *in vivo*, indicating that these cells were proliferating (data not shown). In addition, using *in vitro* clonal differentiation assays[11], *mkk7*$^{-/-}$ and *mkk7*$^{+/-}$ precursors derived from the liver of E10.5 embryos developed into macrophages/monocytes, mast cells and immunoglobulin-secreting B lymphocytes (data not shown). Thus, haematopoietic precursors present in *mkk7*$^{-/-}$ liver remnants can give rise to various haematopoietic cell lineages. In contrast, proliferation of hepatocytes was markedly impaired in E11.5 *mkk7*$^{-/-}$ embryos, as determined by BrdU *in vivo* labelling (data not shown). Reduced proliferation of hepatocytes was also observed in primary hepatocyte cultures isolated from *mkk7*$^{-/-}$ E11.5 embryos (Fig. 4e). JNK activation was abolished in these primary *mkk7*$^{-/-}$ hepatocytes in response to hepatocyte growth factor (HGF) treatment (Fig. 4f). Similarly to *mkk7*$^{-/-}$ MEFs, *cdc2* mRNA expression was downregulated in primary *mkk7*$^{-/-}$ hepatocytes (Fig. 4g). Thus, these results suggest that the MKK7–JNK signalling pathway is important for CDC2 expression, and proliferation of MEFs and primary hepatocytes.

CDC2 is a target for MKK7–JNK signalling

Reduced CDC2 expression in *mkk7*$^{-/-}$ MEFs could be an indirect consequence of premature senescence, or CDC2 could be a direct target of the MKK7–JNK signalling pathway. MKK7 or JNK was not co-immunopreciptated with CDC2/ cyclin B1 and phosphorylation of CDC2/ cyclin B1 by recombinant MKK7 or recombinant JNK was not observed using *in vitro* kinase assays (data not shown). *In silico* analysis of the murine *cdc2* promoter region identified several predicted AP-1 elements in the −3,440 to +1 bp region (Fig. 5a, asterisks). Luciferase promoter assays using deletion mutants in phoenixE cells showed that the sequence 5′-AGAGTCA-3′ at −184/−178 of the *cdc2* promoter is a potential AP-1 site required for effective *cdc2* transactivation (Fig. 5a). It should be noted that the identical promoter sequence has been previously identified in the prostaglandin G/H synthase-2 promoter[29]. Treatment with TPA (12-*O*-tetradecanoylphorbol-13-acetate) and serum induce binding to oligonucleotides containing the 5′-AGAGTCA-3′ sequence, and antibodies specific for c-Jun and c-Fos inhibit binding of AP-1 to the prostaglandin G/H synthase-2 promoter in electromobility shift assays (EMSAs) [29]. Mutation of the *cdc2* AP-1 site rendered lower promoter transactivation in our luciferase assays, albeit to a lesser extent than a mutation in the previously defined[30] *cdc2* promoter −129/−121 E2F-binding site (Fig. 5b). Whether additional AP-1 sites are critical in the CDC2 promoter remains to be determined. Furthermore, transactivation of a *cdc2*-promoter–luciferase reporter construct was impaired in *mkk7*$^{-/-}$ MEFs (Fig. 5c).

In EMSA assays (Fig. 5d), both the consensus AP-1 site and the 5′-AGAGTCA-3′ AP-1 site present in the cdc2 promoter showed band shifts after incubation in serum and UV stimulation. Mutation of the −184/−178 *cdc2* AP-1 site abolished the band shift (Fig. 5d). To determine whether c-Jun, the downstream target of MKK7–JNK, can bind to the *cdc2* promoter region under physiological conditions, chromatin immunoprecipitation (ChIP) analysis was performed (Fig. 5e). The *cdc2* promoter region encompassing the −184/−178 AP-1 site was precipitated in the presence of an anti-c-Jun specific antibody, indicating that c-Jun can bind to the *cdc2* promoter but does not bind to the control *prim1* gene promoter region present on the same chromosome (Fig. 5e). Binding of c-Jun to the *cdc2* promoter in ChIP experiments was confirmed by radioactive PCR (Fig. 5f). To test whether CDC2 is important for cell proliferation in *mkk7*$^{-/-}$ MEFs, wild-type CDC2 was over-expressed. Ectopic expression of wild-type CDC2 in *mkk7*$^{-/-}$ MEFs partially restored proliferation (Fig. 5g). These data identify CDC2 as a target of the MKK7–JNK signalling pathway and indicate that CDC2 might be important for overcoming the cell cycle block of *mkk7*-null cells. However, we cannot rule out the possibility that CDC2 expression might also be controlled indirectly by other MKK7–JNK–c-Jun-regulated molecules, as the direct effect of c-Jun on *cdc2* promoter activity is not strong.

Control of CDC2 expression, senescence and G2/M progression by c-Jun

The MKK7–JNK stress pathway regulates gene transcription through phosphorylation of multiple transcription factors, including c-Jun or ELK-1 (refs 1–5). As we observed reduced phosphorylation and expression of c-Jun in *mkk7*$^{-/-}$ fibroblasts (Fig. 4a), and c-Jun controls the *cdc2* promoter (Fig. 5), we wanted to confirm the role of c-Jun in cellular senescence, G2/M progression and CDC2 expression in genetic experiments.

Consistent with the impaired phosphorylation of c-Jun and reduced CDC2 expression in *mkk7*$^{-/-}$ MEFs, *c-jun*$^{-/-}$ MEFs also displayed reduced expression of CDC2 protein at later passages (Fig. 6a). Importantly, MEFs derived from *c-junAA* mutant mice carrying a mutant of both c-Jun phosphorylation sites[13,14] also showed reduced CDC2 protein (Fig. 6a), as well as reduced *cdc2* mRNA expression after more than five passages (Fig. 6b). Over-expression of c-Jun in *mkk7*$^{-/-}$ MEFs restored CDC2 expression (Fig. 6c) and transactivation of the *cdc2* AP-1 promoter construct to levels observed in wild-type MEFs (Fig. 6d). Activity of the *cdc2* promoter construct was also reduced in *c-junAA* MEFs (Fig. 6e). Moreover, in EMSA experiments binding of MEF extracts to consensus AP-1 and *cdc2* AP-1 oligonucleotides were reduced in both *mkk7*$^{-/-}$ and *c-junAA* MEFs (Fig. 6f). These data show

that CDC2 expression can be regulated by the MKK7–JNK–c-Jun signalling pathway.

To evaluate whether c-Jun controls G2/M progression, cell-cycle analysis was performed in early passage *c-jun*$^{-/-}$ and *c-junAA* MEFs. Similarly to *mkk7*$^{-/-}$ MEFs, loss of c-Jun or inactivation of the JNK phosphorylation sites of c-Jun resulted in the accumulation of cells at the G2/M boundaries beginning from passage 4 (Table 2). Immunostaining with phospho-Histone H3 confirmed that the arrest occurred at the G2 phase, rather than the M phase (Fig. 7a). Importantly, over-expression of c-Jun rescued the defects in proliferation and premature senescence observed in *mkk7*$^{-/-}$ MEFs (Fig. 7b–d). These data suggest an involvement of the MKK7–JNK–c-Jun pathway in G2/M cell cycle progression and cell proliferation in MEFs.

DISCUSSION

Our results show that MKK7 and c-Jun are critical for MEF proliferation and G2/M cell-cycle progression. Previous data from other groups have shown that the JNK–c-Jun signalling pathway is required to promote proliferation in primary MEFs[17,19,32]. However, it has been shown recently that JNK1/JNK2 signalling may attenuate proliferation after Ras-mediated transformation in 3T3 cells[32]. It should be noted that overexpression of Ras causes premature cellular senescence in primary MEFs, whereas it can transform most immortalized cells (such as 3T3 MEFs) in the presence of inactive tumour suppressors such as p53 or p16 (ref. 33) during long-term cell culture. Thus, the different genetic background and treatments might determine the different outcomes. Our genetic and biochemical data clearly show that in non-transformed primary MEFs, as well as embryonic liver cells, MKK7 is a crucial kinase for cell proliferation. In contrast, it has been shown that MKK7 is a negative regulator of haematopoietic cell proliferation[12,34]. The *in vitro* growth behaviours of haematopoietic cells are different from other cell types, and the role of MKK7–JNK in haematopoietic cells has only been studied under basal conditions. Thus, it would be interesting to determine the growth behaviours of such cells under conditions of stress, such as low population densities or altered serum condition. In addition, it is possible that MKK7 might regulate additional pathways.

One intriguing aspect of our results is that early passage *mkk7*$^{-/-}$ MEFs behave similarly to wild-type cells, but then rapidly down-regulate CDC2 expression and display premature senescence and defective proliferation. Similarly, proliferation of primary hepatocytes in *mkk7*$^{-/-}$ embryos seems to be normal in early foetal development, followed by downregulation of CDC2 and defective proliferation. In cell culture, it has been shown that conditions of stress, such as low serum or low cell densities, trigger premature senescence in wild-type fibroblasts and many other cell types[35]. Thus, it seems that under conditions of environmental stress and possibly during certain developmental processes such as liver formation, the MKK7–JNK–c-Jun pathway might function to upregulate CDC2 expression and maintain the proliferative state of the cells. Determination of cell fates by MKK7–JNK–c-Jun-induced CDC2 expression might explain why loss of MKK7 results in premature senescence and a G2/M cycle arrest, whereas the cells that express MKK7 undergo crisis at much later stages and predominantly arrest at G1 phase. Our results provide a molecular link between environmental stresses, premature senescence and G2/M cell-cycle progression. Whether MKK7–JNK-c-Jun signalling is involved in the regulation of molecules previously known to be involved in senescence needs to be determined. To investigate the connection to p53 (ref. 36) further, we generated *p53*$^{-/-}$*mkk7*$^{-/-}$ MEFs and observed rescue of CDC2 expression and cellular senescence, as well as restored proliferation. Thus, p53 is also important for the process. In addition, some other molecules controlled by the MKK7–JNK–c-Jun pathway might also be involved in the regulation of CDC2 expression at transcriptional, translational and post-translational levels, as it has been shown that *cdc2* transactivation is regulated by multiple mechanisms depending on cell types[37] and that c-Jun can control a variety of molecules such as E2F[19].

It has been suggested that the mechanisms regulating the cell cycle also have a role in apoptosis[38]. The induction of proteins that control G1/S transition in proliferating cells occurs in dying neurons[39], and G1 cyclin-dependent kinases seem to trigger neuronal cell death[40]. Moreover, E2F1-1 and CDK2 seem to control thymocyte apoptosis[41,42]. The G2/M cell-cycle regulator CDC2 induces phosphorylation of the BH3-only protein BAD and triggers neuronal apoptosis[43]. This notion is consistent with our results on the normal susceptibility to cell death in CDC2-expressing *mkk7*$^{-/-}$ MEFs, but the resistance to death triggers in *mkk7*$^{-/-}$ 3T3 cells that express low levels of CDC2. Furthermore, we showed that overexpression of constitutively active CDC2 in wild-type and *mkk7*$^{-/-}$ MEFs results in cell death (data not shown). Thus, regulation of CDC2 by stress kinases might be also involved in stress-kinase-regulated cell death. The role of JNKs in cell death has been controversial and is dependent on the experimental system used. Our results in MEF apoptosis experiments indicate that the MKK7–JNK–c-Jun pathway determines the molecular history of cells, and this is a critical determinant for cell death. Whether stress kinases also set the molecular switches for cell death susceptibility in other cell types remains to be determined.

Our results show that MKK7 is essential for embryogenesis and liver development. Loss of MKK7 in fibroblasts results in impaired proliferation, premature senescence and a G/2M cell-cycle arrest. We identified the G2/M kinase CDC2 as a molecular target for the MKK7–JNK–c-Jun signalling pathway. These data provide a new paradigm by which the MKK7–JNK–c-Jun signalling pathway couples developmental and environmental cues to proliferation, G2/M cycle arrest and cellular senescence. □

METHODS

Gene targeting. To disrupt the murine *mkk7* gene in embryonic stem cells, a portion of exon 9, including the phosphorylation motif, was replaced with a PGK-Neo cassette (see Supplementary information, Fig. S1a), as described previously[34]. *c-Jun* and *c-JunAA* mutant mice and MEFs have been described previously[13,19]. All mice were kept at the Ontario Cancer Institute and IMP animal facilities in accordance with institutional guidelines.

MEF and hepatocyte cultures. MEFs were prepared from E11.5 embryos and maintained in DMEM contatining 10% foetal calf serum (FCS). Cell proliferation in all MEFs was determined using WST-1 (Roche, Indianapolis, IN). The percentage of cells in each phase of the cell cycle was calculated with ModiFit software (Becton Dickinson, Oakville, Canada). Population doubling curves were determined using trypan-blue exclusion. For detection of apoptosis, MEFs were stained with annexin V/propidium iodide (PI) using an apoptosis detection kit (R&D Systems, Minneapolis, MN). For cell-cycle analysis, MEFs were fixed with 70% ethanol, labelled with PI and analysed by FACS. All samples were analysed by flow cytometry. Protein expression levels were determined using antibodies specific to p16, p21, cyclin D1, cyclin B1, MKK4, JNKs, p38-MAPK, ATF2, c-Jun, phospho-c-Jun, JunB, JunD (antibodies were purchased from Santa Cruz Biotechnology, Santa Cruz, CA), p53 (Novacastra, distributed by Vecter Laboratories, Burlingame, CA), CDC2 and ERK1/2 (Cell Signaling, Beverly, MA). For primary hepatocyte cultures, haematopoietic cells were depleted using antibodies to CD45 and TER119. The remaining parenchymal liver cells were cultured for 2 days, and cell proliferation was determined using WST-1 (Roche). *cdc2* mRNA expression was detected with a full-length CDC2 cDNA probe or RT-PCR. JNK activity in mouse embryonic liver was determined as described[44].

Expression assays. For ectopic gene expression, the retroviral vectors pBabe-puro, pBabe-puro-Flag-MKK7, pBabe-puro-MKK4, pBabe-puro-c-Jun or

pBabe-puro-CDC2 (wild-type) were transfected into a phoenix-E packaging cell line. MEFs were cultured in the supernatant of the packaging cells for 1 day and selected with 2.5 mg ml^{-1} puromycin for 2 days before recovery for a further 2 days. Empty pBabe-puro vectors did not have any detectable effect on the phenotype of MEFs.

Detection of senescent cells and cell staining. SA-β-gal staining was performed using a senescence staining kit (Cell Signaling). For Phalloidin–rhodamine/DAPI staining, SA-β-gal-stained cells were fixed, treated with 0.1% Triton X-100/3% skimmed milk/TBS and double-stained with phalloidin–rhodamine (Sigma, St Louis, MO) and DAPI (Molecular Probes, Eugene, OR). All SA-β-gal-positive cells had the typical flattened cell morphology determined by phalloidin/DAPI staining. Phospho-Histone H3 was determined using a phosphorylation (Ser 10)-specific antibody (Cell Signaling).

Promoter assays. The full-length CDC2 promoter was cloned from mouse genomic DNA using PCR, and the sequence was confirmed. The promoter constructs were transfected into Phoenix E cells or *mkk7*$^{+/-}$ and *mkk7*$^{-/-}$ MEFs, and luciferase activity was determined using a Luciferase Assay Kit (Promega, Madison, WI). For EMSAs, cell extracts were harvested from 5×10^6 cells according to standard protocols. Briefly, protein extracts (1 μg) were incubated in 20 μl binding buffer with end-labelled, double-stranded, oligonucleotide probes (consensus AP-1: 5′-CGCTTGATGACTCAGCCGGAA-3′; CDC2 promoter AP-1 site: 5′-AACAGAGCTCAAGAGTCAGTTGG-3′; mutant CDC2 promoter AP1 site: 5′-AACAGAGCTCAAGATCTAGTTGG-3′) and fractionated on a 5% polyacrylamide gel. The binding buffer was: 10 mM Hepes-HCl at pH 7.9, 100 mM potassium chloride, 0.5 mM magnesium chloride, 0.1 mM EDTA, 0.5 mM dithiothreitol, 2 μg poly (dI-dC) and 10% glycerol. Chromatin immunoprecipitations (ChIPs) were performed as described[45]. The sequences of the ChIP primers were 5′-CTGTCACTTTGGTGGCTGGC-3′ and 5′-TCCGACTCACGCCATACCTC-3′ for *cdc2*; 5′-GTCAGCATCTAGCACACAGGTCC-3′ and 5′-GAAATCCAGGTAGGGTTCCAGG-3′ for *prim1*.

Kinase assays. To detect JNK and p38-MAPK activities, JNK proteins were immunoprecipitated at 4 °C using anti-JNK antibodies (C-17; Santa Cruz). Kinase activities were determined using glutathione *S*-transferase (GST)–c-Jun as a substrate in the presence of 50 μM γ-^{32}P-ATP. The amount of total JNK protein in the immunoprecipitated lysates were determined by Western blotting. cyclinB1/CDC2 kinase activities were determined by anti- cyclinB1 immunocomplex kinase assays using Histone H1 (HH1) as substrate.

Note: Supplementary Information is available on the Nature Cell Biology website.

ACKNOWLEDGMENTS

We thank J. Woodgett, L. Harrington, J. C. Zuniga-Pflucker, T. Schmitt, J. Joza, C. Krawczyk, E. Griffith, L. Barra, M. Crackower, U. Erickson, L. Zhang, H. Hara and M. Rangachari for discussion and reagents. T.W. is supported by the H15th fellowship of the Japan Society for the Promotion of Science. This work is supported by the National Cancer Institute of Canada (NCIC), the Institute of Molecular Biotechnology of the Austrian Academy of Sciences (IMBA), and the Jubilaeumsfonds of the Austrian National Bank.

COMPETING FINANCIAL INTERESTS

The authors declare that they have no competing financial interests.

Received 26 June 2003; accepted 28 January 2004
Published online at http://www.nature.com/naturecellbiology.

1. Chang, L. & Karin, M. Mammalian MAP kinase signalling cascades. *Nature* **410**, 37–40 (2001).
2. Seger, R. & Krebs, E. G. The MAPK signaling cascade. *FASEB J.* **9**, 726–735 (1995).
3. Tibbles, L. A. & Woodgett, J. R. The stress-activated protein kinase pathways. *Cell Mol. Life Sci.* **55**, 1230–1254 (1999).
4. Waskiewicz, A. J. & Cooper, J. A. Mitogen and stress response pathways: MAP kinase cascades and phosphatase regulation in mammals and yeast. *Curr. Opin. Cell Biol.* **7**, 798–805 (1995).
5. Davis, R. J. Signal transduction by the JNK group of MAP kinases. *Cell* **103**, 239–252 (2000).
6. Roovers, K. & Assoian, R. K. Integrating the MAP kinase signal into the G1 phase cell cycle machinery. *Bioessays* **22**, 818–826 (2000).
7. Johnson, G. L. & Lapadat, R. Mitogen-activated protein kinase pathways mediated by ERK, JNK, and p38 protein kinases. *Science* **298**, 1911–1912 (2002).
8. Kishimoto, H. *et al.* Different properties of SEK1 and MKK7 in dual phosphorylation of stress-induced activated protein kinase SAPK/JNK in embryonic stem cells. *J. Biol. Chem.* **278**, 16595–16601 (2003).
9. Wada, T. *et al.* Impaired synergistic activation of stress-activated protein kinase SAPK/JNK in mouse embryonic stem cells lacking SEK1/MKK4: different contribution of SEK2/MKK7 isoforms to the synergistic activation. *J. Biol. Chem.* **276**, 30892–30897 (2001).
10. Fleming, Y. *et al.* Synergistic activation of stress-activated protein kinase 1/c-Jun N-terminal kinase (SAPK1/JNK) isoforms by mitogen-activated protein kinase kinase 4 (MKK4) and MKK7. *Biochem J.* **352**, 145–154 (2000).
11. Nishina, H. *et al.* Defective liver formation and liver cell apoptosis in mice lacking the stress signaling kinase SEK1/MKK4. *Development* **126**, 505–516 (1999).
12. Dong, C. *et al.* JNK is required for effector T-cell function but not for T-cell activation. *Nature* **405**, 91–94 (2000).
13. Behrens, A., Sibilia, M. & Wagner, E. F. Amino-terminal phosphorylation of c-Jun regulates stress-induced apoptosis and cellular proliferation. *Nature Genet.* **21**, 326–329 (1999).
14. Behrens, A., Jochum, W., Sibilia, M. & Wagner, E. F. Oncogenic transformation by ras and fos is mediated by c-Jun N-terminal phosphorylation. *Oncogene* **19**, 2657–2663 (2000).
15. Tournier, C. *et al.* MKK7 is an essential component of the JNK signal transduction pathway activated by proinflammatory cytokines. *Genes Dev* **15**, 1419–1426 (2001).
16. Hochedlinger, K., Wagner, E. F. & Sabapathy, K. Differential effects of JNK1 and JNK2 on signal specific induction of apoptosis. *Oncogene* **21**, 2441–2445 (2002).
17. Tournier, C. *et al.* Requirement of JNK for stress-induced activation of the cytochrome *c*-mediated death pathway. *Science* **288**, 870–874 (2000).
18. Dimri, G. P. *et al.* A biomarker that identifies senescent human cells in culture and in aging skin *In vivo*. *Proc. Natl Acad. Sci. USA* **92**, 9363–9367 (1995).
19. Schreiber, M. *et al.* Control of cell cycle progression by c-Jun is p53 dependent. *Genes Dev.* **13**, 607–619 (1999).
20. Sherwood, S. W., Rush, D., Ellsworth, J. L. & Schimke, R. T. Defining cellular senescence in IMR-90 cells: a flow cytometric analysis. *Proc. Natl Acad. Sci. USA* **85**, 9086–9090 (1988).
21. Paulson, J. R., Taylor, S. S., Lake, R. S. & Salzman, N. P. Phosphorylation of histones 1 and 3 and nonhistone high mobility group 14 by an endogenous kinase in HeLa metaphase chromosomes. *J. Biol. Chem.* **257**, 6064–6072 (1982).
22. Lake, R. S. & Salzman, N. P. Occurrence and properties of a chromatin-associated F1-histone phosphokinase in mitotic Chinese hamster cells. *Biochemistry* **11**, 4817–4826 (1972).
23. Bulavin, D. V. *et al.* Initiation of a G2/M checkpoint after ultraviolet radiation requires p38 kinase. *Nature* **411**, 102–107 (2001).
24. Shackelford, R. E., Kaufmann, W. K. & Paules, R. S. Cell cycle control, checkpoint mechanisms, and genotoxic stress. *Environ. Health Perspect.* **107**, 5–24 (1999).
25. Orren, D. K., Petersen, L. N. & Bohr, V. A. A UV-responsive G2 checkpoint in rodent cells. *Mol. Cell. Biol.* **15**, 3722–3730 (1995).
26. Toussaint, O. *et al.* Stress-induced premature senescence. Essence of life, evolution, stress, and aging. *Ann. NY Acad. Sci.* **908**, 85–98 (2000).
27. Th'ng, J. P. *et al.* The FT210 cell line is a mouse G2 phase mutant with a temperature-sensitive CDC2 gene product. *Cell* **63**, 313–324 (1990).
28. Arion, D., Meijer, L., Brizuela, L. & Beach, D. *cdc2* is a component of the M phase-specific histone H1 kinase: evidence for identity with MPF. *Cell* **55**, 371–378 (1988).
29. Okada, Y., Voznesensky, O., Herschman, H., Harrison, J. & Pilbeam, C. Identification of multiple *cis*-acting elements mediating the induction of prostaglandin G/H synthase-2 by phorbol ester in murine osteoblastic cells. *J. Cell. Biochem.***78**, 197–209 (2000).
30. Dalton, S. Cell cycle regulation of the human cdc2 gene. *EMBO J.* **11**, 1797–1804 (1992).
31. Kovary, K. & Bravo, R. The jun and fos protein families are both required for cell cycle progression in fibroblasts. *Mol. Cell. Biol.* **11**, 4466–4472 (1991).
32. Kennedy, N. J. *et al.* Suppression of Ras-stimulated transformation by the JNK signal transduction pathway. *Genes Dev.* **17**, 629–637 (2003).
33. Serrano, M., Lin, A. W., McCurrach, M. E., Beach, D. & Lowe, S. W. Oncogenic ras provokes premature cell senescence associated with accumulation of p53 and p16INK4a. *Cell* **88**, 593–602 (1997).
34. Sasaki, T. *et al.* The stress kinase mitogen-activated protein kinase kinase (MKK)7 is a negative regulator of antigen receptor and growth factor receptor-induced proliferation in hematopoietic cells. *J. Exp. Med.* **194**, 757–768 (2001).
35. Didinsky, J. B. & Rheinwald, J. G. Failure of hydrocortisone or growth factors to influence the senescence of fibroblasts in a new culture system for assessing replicative lifespan. *J. Cell. Physiol.* **109**, 171–179 (1981).
36. Wynford-Thomas, D. p53: guardian of cellular senescence. *J. Pathol.* **180**, 118–121 (1996).
37. Sugarman, J. L., Schonthal, A. H. & Glass, C. K. Identification of a cell-type-specific and E2F-independent mechanism for repression of cdc2 transcription. *Mol. Cell. Biol.* **15**, 3282–3290 (1995).
38. King, K. L. & Cidlowski, J. A. Cell cycle and apoptosis: common pathways to life and death. *J. Cell. Biochem.* **58**, 175–180 (1995).
39. Freeman, R. S., Estus, S. & Johnson, E. M. Jr. Analysis of cell cycle-related gene expression in postmitotic neurons: selective induction of cyclin D1 during programmed cell death. *Neuron* **12**, 343–355 (1994).
40. Park, D. S. *et al.* cyclin-dependent kinases participate in death of neurons evoked

by DNA-damaging agents. *J. Cell Biol.* **143**, 457–467 (1998).
41. Hakem, A., Sasaki, T., Kozieradzki, I. & Penninger, J. M. The cyclin-dependent kinase Cdk2 regulates thymocyte apoptosis. *J. Exp. Med.* **189**, 957–968 (1999).
42. Field, S. J. *et al.* E2F-1 functions in mice to promote apoptosis and suppress proliferation. *Cell* **85**, 549–561 (1996).
43. Konishi, Y., Lehtinen, M., Donovan, N. & Bonni, A. Cdc2 phosphorylation of BAD links the cell cycle to the cell death machinery. *Mol. Cell* **9**, 1005–1016 (2002).
44. Watanabe, T. *et al.* SEK1/MKK4-mediated SAPK/JNK signaling participates in embryonic hepatoblast proliferation via a pathway different from NF-κB-induced anti-apoptosis. *Dev. Biol.* **250**, 332–347 (2002).
45. Weinmann, A. S., Bartley, S. M., Zhang, T., Zhang, M. Q. & Farnham, P. J. Use of chromatin immunoprecipitation to clone novel E2F target promoters. *Mol. Cell Biol.* **21**, 6820–6832 (2001).

Transplantation of Bone Marrow Cells Reduces CCl_4-Induced Liver Fibrosis in Mice

Isao Sakaida,[1] Shuji Terai,[1] Naoki Yamamoto,[1] Koji Aoyama,[1] Tsuyoshi Ishikawa,[1] Hiroshi Nishina,[2] and Kiwamu Okita[1]

We investigated the effect of bone marrow cell (BMC) transplantation on established liver fibrosis. BMCs of green fluorescent protein (GFP) mice were transplanted into 4-week carbon tetrachloride (CCl_4)–treated C57BL6 mice through the tail vein, and the mice were treated for 4 more weeks with CCl_4 (total, 8 weeks). Sirius red and GFP staining clearly indicated migrated BMCs existing along with fibers, with strong expression of matrix metalloproteinase (MMP)-9 shown by anti–MMP-9 antibodies and *in situ* hybridization. Double fluorescent immunohistochemistry showed the expression of MMP-9 on the GFP-positive cell surface. Film *in situ* zymographic analysis revealed strong gelatinolytic activity in the periportal area coinciding with the location of MMP-9–positive BMCs. Four weeks after BMC transplantation, mice had significantly reduced liver fibrosis, as assessed by hydroxyproline content of the livers, compared to that of mice treated with CCl_4 alone. Subpopulation of Liv8-negative BMCs was responsible for this fibrolytic effect. In conclusion, mice with BMC transplants with continuous CCl_4 injection had reduced liver fibrosis and a significantly improved survival rate after BMC transplantation compared with mice treated with CCl_4 alone. This finding introduces a new concept for the therapy of liver fibrosis. *Supplementary material for this article can be found on the HEPATOLOGY website (http://interscience.wiley.com/jpages/0270-9139/suppmat/index.html).* (HEPATOLOGY 2004;40: 1304–1311.)

Recent reports have shown the capacity of the bone marrow cell (BMC) to differentiate into a variety of non-hematopoietic cell lineages.[1–5] These results indicate that the BMC is an attractive cell source for regenerative medicine compared with tissue-specific stem cells.[6] The capacity of the BMC to differentiate into hepatocytes and intestinal cells has been shown by Y-chromosome detection in autopsy analysis of human female recipients of BMCs from male donors.[7,8] Although Lagasse et al. reported that purified hematopoietic stem cells could differentiate into hepatocytes using a fumarylacetate hydrase-deficient model,[5] Wagers et al. showed little evidence of plasticity in adult hematopoietic stem cells.[9] Thus, although there is still controversy about which part of BMCs can differentiate into hepatocytes, the BMC seems to have the plasticity to differentiate into such cells. From the point of view of therapy, one of the targets of liver disease for BMC transplantation is liver cirrhosis with chronic liver failure. This is an unphysiological condition with excessive deposition of extracellular matrix and a relative lack of parenchymal cells (hepatocytes). Even if BMC transplantation is successful in supplying parenchymal cells, the fate of the extracellular matrix under these conditions is unknown. The present study clearly shows that transplanted BMCs reduce (degrade) carbon tetrachloride (CCl_4)-induced liver fibrosis with a significantly improved survival rate.

Materials and Methods

Mice. GFP-transgenic mice (TgN(β-act-EGFP)Osb) were kindly provided by Masaru Okabe (Genome Research Center, Osaka University, Osaka, Japan).[10] C57BL6 female mice were purchased from Japan SLC

Abbreviations: BMC, bone marrow cell; CCl4, carbon tetrachloride; GFP, green fluorescent protein; PBS, phosphate-buffered saline; IgG, immunoglobulin G; MMP, matrix metalloproteinase; NGS, normal goat serum; NRS, normal rabbit serum; DIG, digoxigenin.

From the [1]Department of Gastroenterology and Hepatology, School of Medicine, Yamaguchi University, Yamaguchi, Japan; and [2]Department of Physiological Chemistry, Graduate School of Pharmaceutical Science, University of Tokyo, Tokyo, Japan.

Received September 30, 2003; accepted August 16, 2004.

Supported in part by grants-in-aid 16590597, 12670490, and 10470136 from the Ministry of Education, Culture, Sports, Science and Technology and by grants-in-aid for translational research from the Ministry of Health, Labor and Welfare of Japan.

Address reprint requests to: Isao Sakaida, M.D., Department of Gastroenterology and Hepatology, School of Medicine, Yamaguchi University, Minami-Kogushi 1-1-1 Ube, Yamaguchi-pref. 755-8505, Japan. E-mail: sakaida@yamaguchi-u.ac.jp; fax: (81) 836-22-2240.

Published online in Wiley InterScience (www.interscience.wiley.com).

DOI 10.1002/hep.20452

(Shizuoka, Japan). Mice were properly anesthetized during experiments.

Experimental Protocol. Six-week-old female C57BL6 mice were treated with 1 mL/kg CCl_4 dissolved in olive oil (1:1) twice a week for 4 weeks. One day (24 hours) after the eighth injection of CCl_4, 1×10^5 green fluorescent protein (GFP)-positive BMCs or sorted Liv8-positive or Liv8-negative BMCs (1×10^5 cells) or same volume of saline as a control (described also as mice treated with CCl_4 alone) were injected into the tail vein as described previously.[11,12] Mice continued to be treated with CCl_4. After 1, 2, 3, or 4 weeks, mice were then sacrificed to assess the extent of liver fibrosis. For examination of the survival rate, mice were treated with CCl_4 for 4 weeks and divided into 2 groups (15 mice each) with bone marrow transplantation or the same volume of saline injection. All mice were then treated with CCl_4 for a further 25 weeks.

BMC Preparation. For BMC isolation, GFP-transgenic mice (TgN(β-act-EGFP)Osb) (6 weeks old) were killed by cervical dislocation and the limbs removed. GFP-positive BMCs were flushed with Dulbecco's Modified Eagle medium (DMEM) culture medium with 10% fetal bovine serum (FBS) from the medullary cavities of tibias and femurs using a 25-G needle.

Production of Rat Monoclonal Antibody, Liv8. Eight-week old WKY/NCrj female rats were immunized in the hind footpads with 100 μg of E11.5 murine fetal liver lysate in complete Freund's adjuvant (0.2 mL). Anti-Liv8 antibodies were raised according to a previously described protocol.[13]

Fluorescence-Activated Cell Sorter Analysis of Fetal Liver Cells and BMCs Using Anti-Liv8 Antibody. Prepared mouse fetal liver cells (E11.5) and adult BMCs were reacted with biotin-conjugated anti-Liv8 antibody,[12] phycoerythrin-conjugated rat anti-CD45 (Becton Dickinson Bioscience, San Jose, CA), fluorescein isothiocyanate-conjugated anti–c-kit (Becton Dickinson Bioscience), phycoerythrin-conjugated anti–Thy 1 (Becton Dickinson Bioscience), and fluorescein isothiocyanate-conjugated anti-B220 antibodies (Becton Dickinson Bioscience) at the rate of 1 μg per 10^6 total cells, mixed well, and incubated in the tube for 30 to 40 minutes at 4°C. Following the incubation with the first antibody, the cells were washed twice by 0.02 mol/L phosphate-buffered saline (PBS) and centrifuged at 500*g* for 5 minutes. Labeled cells were then reacted to allophycocyanin-conjugated streptavidin (Becton Dickinson Bioscience) at the rate of 1 μg per 10^6 total cells, mixed well, and incubated in the tube for 30 to 40 minutes at 4°C. After that, these were washed out once with 0.02 mol/L PBS and centrifuged at 500*g* for 5 minutes. The labeled cells were analyzed using FACS Calibur (Becton Dickinson Bioscience).

Preparation of Liv8-positive and Liv8-negative BMCs Liv8-positive and Liv8-negative BMCs were prepared as described previously.[12] Briefly, prepared BMCs were reacted to rat anti-Liv8 immunoglobulin G (IgG) antibody at the rate of 1 μg per 10^6 total cells, mixed well, and incubated in the tube for 30 minutes at 4°C. Cells were then washed twice by 0.02 mol/L PBS and centrifuged at 500*g* for 5 minutes. Cells were labeled with rat anti-Liv8 IgG antibody by reacting with goat anti-rat IgG MicroBeads (Miltenyi Biotec GmbH, Bergisch Gladbach, Germany) at the rate of 20 μL per 10^7 total cells, mixed well, and incubated for 20 minutes at 4°C. Labeled cells were washed once by 0.02 mol/L PBS and centrifuged at 500*g* for 5 minutes. These cells were separated into Liv8-positive cells or Liv8-negative cells by the autoMACS magnetic cell sorting system (Miltenyi Biotec GmbH) for 10 minutes per tube.

Tissue Preparation and Immunohistochemistry. The liver was perfused via the heart with 4% paraformaldehyde to flush out blood cells and incubated with 4% paraformaldehyde overnight. Tissues were then soaked in 30% sucrose for 3 days. Tissues were frozen with liquid nitrogen to prepare for sectioning with a cryostat for immunohistochemistry.

Cells expressing GFP and matrix metalloproteinase (MMP)-9 (or α-smooth muscle actin) were analyzed by both fluorescent microscopy and conventional immunohistochemistry using anti-GFP, anti–MMP-9 (Santa Cruz Biotechnology, Santa Cruz, CA), and anti–α-smooth muscle actin antibodies (Sigma-Aldrich, St. Louis, MO). Tissues were soaked in 0.3% Triton X-100 with 0.05% normal goat serum (NGS) (Chemicon, Temecula, CA) or normal rabbit serum (NRS) (Chemicon) in PBS overnight. The next day, the tissues were put in 500 mL of 10% NGS or NRS in 0.3% Triton X-100 of PBS for 2 hours, then washed with 0.3% Triton X-100 with 0.05% NGS or NRS in PBS for 10 minutes. We soaked the tissues in 1.5% H_2O_2 in 50% methanol with distilled water for 2 hours. The tissues were then washed in 0.3% Triton X-100 with 0.05% NGS or NRS in PBS. Sections were incubated with anti-GFP and anti–MMP-9 (ICN Pharmaceuticals Inc., Kanagawa, Japan) antibodies. Anti–biotin-conjugated anti-goat IgG, anti-rabbit IgG, biotin-conjugated rabbit anti-goat IgG, and biotin-conjugated rabbit anti-mouse IgG were purchased from Dako Japan (Kyoto, Japan) and used as the secondary antibodies. PAP-goat (B0157), PAP-mouse (B0650), and PAP-rabbit (Z0113) polyclonal antibodies (Dako Japan) were used as third antibodies.

For fluorescent immunohistochemistry, we used Alexa Fluor R 488 and 568 donkey anti–goat- or anti–rabbit-

or anti–mouse-IgG (H + L)-conjugated antibodies (Molecular Probe Inc., Eugene, OR) as second antibodies.

For the evaluation of fibrosis, picro-sirius red staining was performed using 0.1% picro-sirius red solution as previously described.[14]

Quantitative Analysis of Liver Fibrosis. We quantified the liver fibrosis area with picro-sirius red staining using an Olympus Provis microscope equipped with a CCD camera (Tokyo, Japan), as described previously.[15] Briefly, the red area, considered the fibrotic area, was assessed by computer-assisted image analysis with MetaMorph software (Universal Imaging Corporation, Downingtown, PA) at a magnification of ×40. The mean value of 6 randomly selected areas per sample was used as the expressed percent area of fibrosis.

Microarray Analysis. Microarray analysis was performed as described previously.[16]

Briefly, total RNA of liver was isolated using the Atlas Pure Total RNA labeling system (Clontech Laboratories, Inc.) from mice 1 week after BMC transplantation (n = 3) or from mice treated with CCl_4 for 5 weeks (n = 3) according to the manufacturer's recommendations. Differential hybridization analysis was done using an Atlas Mouse complementary DNA expression array (BD Bioscience Clontech, Tokyo, Japan). Complementary DNA probe preparation and hybridization were done according to the manufacturer's recommendations. The array results were scanned with a Strom 840 PhosphoImager (Molecular Dynamics, Sunnyvale, CA) and analyzed with Atlas Image software (BD Bioscience Clontech). The results show the mean values of 3 mice in each group.

Hydroxyproline Content. Hydroxyproline content was determined by a modification of Kivirikko's method, as previously reported.[17] Briefly, liver specimens were weighed, and 20 mg of the freeze-dried sample was hydrolyzed in 6 mol/L HCl at 110°C in an autoclave at a pressure of 1.2 kg force/cm^2 for 24 hours. After centrifugation at 2,000 rpm at a temperature of 4°C for 5 minutes, 2 mL of supernatant was mixed with 50 mL of 1% phenolphthalein and 8 N KOH to obtain a total volume of 5 mL of liquid at pH of 7 to 8. Absorbance was measured at 560 nm. The hydroxyproline content of the liver was expressed as micrograms per gram of wet weight.

In Situ *Hybridization.* *In situ* hybridization was performed essentially as described previously.[18] Briefly, digoxigenin (DIG)-11-UTP–labeled single-stranded RNA probes were prepared with DIG RNA labeling mix and the corresponding T3 or T7 RNA polymerase (Boehringer Mannheim Japan, Tokyo, Japan) according to the manufacturer's instructions. The mouse MMP-9 probe was a 150–base pair fragment from the 3′ untranslated region cloned in the pBluescript (Stratagene, Tokyo, Japan) vector. *In situ* hybridization was performed on tissue sections placed on Superfrost Plus slides postfixed in 4% paraformaldehyde in PBS, rinsed in PBS containing 0.1% active diethyl pyrocarbonate, and prehybridized for 2 hours at 58°C in 50% formamide, 5 × SSC (standard saline citrate), and 40 μg of salmon-sperm DNA per milliliter. Hybridization was carried out at 58°C for 16 hours in a humid chamber with 400 ng of DIG-labeled probe per milliliter diluted in the same solution used for prehybridization. After hybridization, the sections were successively washed in 2 × SSC at room temperature for 30 minutes, 2 × SSC for 1 hour at 65°C, and 0.1 × SSC at 65°C for 1 hour. For the reaction of anti-DIG antibodies, slides were preincubated in buffer A (100 mmol/L Tris, 150 mmol/L NaCl [pH 7.5]), and then with an alkaline phosphatase-coupled anti-DIG antibody (Boehringer Mannheim Japan) diluted 1:5,000 in buffer A containing 0.5% Boehringer blocking reagent for 2 hours at room temperature. The slides were washed in buffer A and then preincubated in buffer C (100 mmol/L Tris, 50 mmol/L $MgCl_2$ [pH 9.5]). Alkaline phosphatase was then revealed as described for 16 to 24 hours at room temperature. The enzymatic reaction was stopped with Tris-ethylenediaminetetraacetic acid (EDTA) for 15 minutes. The slides were rinsed in water for several hours and then dried, cleared in xylene, and mounted directly.

In Situ *Zymography.* *In situ* zymography was performed as described.[19]

The fresh specimens of CCl_4 treated with BMC-transplanted liver tissues (1 week after BMC transplantation) were embedded without fixation in Tissue-Tek optimal cutting temperature compound (Miles, Elkhart, IN). Serial frozen sections were made using a cryostat (MicroM, Walldorf, Germany) and mounted on gelatin films that were coated with 7% gelatin solution (Fuji Photo Film, Tokyo, Japan). The films with sections were incubated for 24 hours at 37°C in a moisture chamber and stained with 1.0% amido black 10B. The gelatin in contact with the proteolytic areas of the sections was digested, and thus zones of enzymic activity were indicated by negative staining. The digested areas in the sections were compared with serial sections stained with hematoxylin-eosin. As a control, liver tissues treated with CCl_4 alone (5 weeks) were used, and the frozen sections were treated in a manner similar to that already described.

Statistical Analysis. Results are presented as the mean ± SD. Differences between groups were analyzed by 1-way ANOVA.

The survival rate was examined using the Breslow-Gehan-Wilcoxon test.

Ethical Considerations. This experiment was reviewed by the Committee of Animal Experiment Ethics at

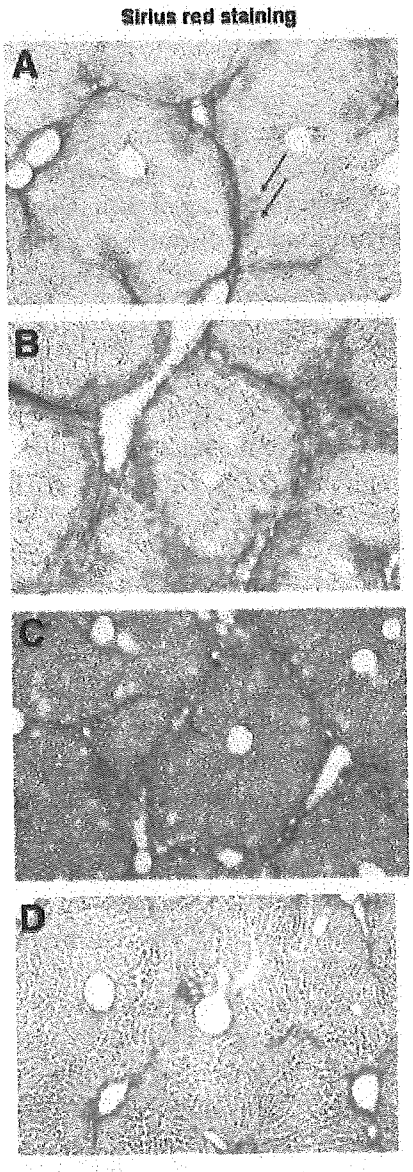

Fig. 1. Photomicrographs of liver sections stained with sirius red from mice after BMC transplantation with continuous CCl_4 treatment. Six-week-old C57BL6 mice were treated with CCl_4 twice a week for 4 weeks. Then, 1×10^5 GFP-positive BMCs were injected through the tail vein. Mice continued to be treated with CCl_4. After (A) 1, (B) 2, (C) 3, and (D) 4 weeks, mice were killed to assess the extent of liver fibrosis. (Original magnification, ×100.)

the Yamaguchi University School of Medicine and was carried out under the guidelines for animal experiments at Yamaguchi University School of Medicine (no. 105).

Results

Five weeks after CCl_4 injection, liver fibrosis was already seen (Supplementary Fig. 1A). One week after BMC transplantation (5 weeks after CCl_4 injection), BMCs were seen along with the fibers recognized by light red staining (black arrows), different from hepatocytes (Fig. 1A) with sirius red staining. More BMCs were seen after 2 weeks (Figs. 1B and 2A,C) and 3 weeks (Figs. 1C and 2B,D), and large spheroid-shaped cells (blue arrows) and small cells (green arrows) (Fig. 2B) were found in the area presumably occupied by fibers (Fig. 2D), shown by sirius red and GFP staining.

Surprisingly, 4 weeks later, the BMC-transplanted liver clearly showed reduction of liver fibrosis (Fig. 1D) compared with the liver treated with CCl_4 alone at 8 weeks (Supplementary Fig. 1D), although CCl_4 was injected throughout the experimental period. Quantitative image analysis of liver fibrosis indicated that the percent area of liver fibrosis at 1 week after BMC transplantation was 5.36% ± 0.90%, but at 4 weeks after transplantation it was significantly decreased to 4.16% ± 0.53% ($P < .001$, n = 8 each; Fig. 3).

Treatment with CCl_4 alone for 8 weeks showed an increased hydroxyproline content of 630 ± 93 μg/wet g liver (Table 1). BMC transplantation significantly reduced this to 392 ± 59 μg/wet g liver 4 weeks later ($P < .01$, n = 8 each). This hydroxyproline content was significantly reduced even compared with that of 1 week after BMC transplantation (494 ± 74 μg/wet g liver, $P < .05$).

The mouse fetal liver at E11.5 functions as a definitive hematopoietic organ, and Liv8-positive cells of the fetal liver at E11.5 include c-kit–positive immature hematopoietic cells and CD45-positive lymphoid cells. These results indicate that almost all Liv8-positive cells are of hematopoietic origin (Supplementary Fig. 2).

In addition, all c-kit–positive mouse adult BMCs belong to the Liv8-positive fraction, and Liv8-positive BMCs include almost all of the CD45- and Thy-1–positive BMCs, in addition to B220, a marker of B lymphocytes (Fig. 4).

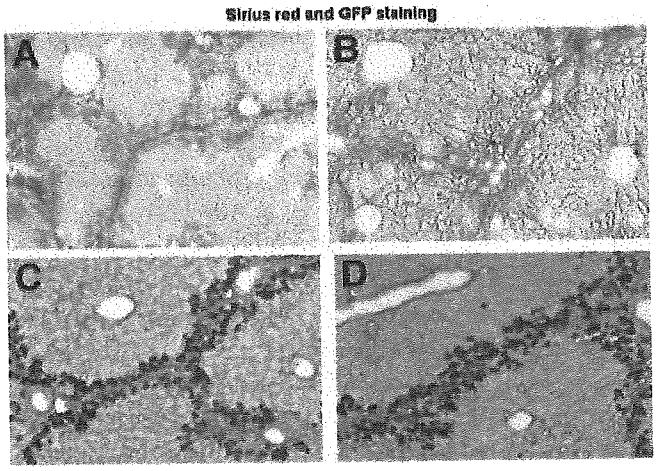

Fig. 2. Photomicrographs of liver sections stained with sirius red or sirius red and GFP from a mouse (A, C) 2 weeks and (B, D) 3 weeks after BMC transplantation. (Original magnification, [A] ×200; [B] ×200; [C] ×200; [D] ×200.)

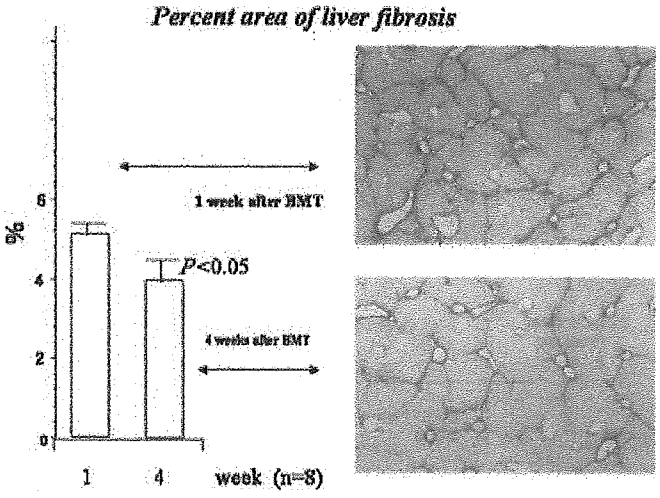

Fig. 3. Quantitatitve analysis of liver fibrosis after bone marrow cell transplantation (BMT). Percent area of liver fibrosis was calculated using sirius red staining as described in Materials and Methods. Results are expressed as mean ± SD of 8 samples. (Original magnification, ×40.)

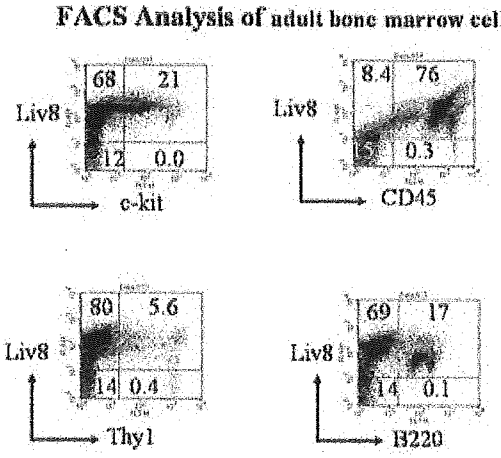

Fig. 4. Expression of Liv8, c-kit, CD45, Thy 1, and B220 in adult BMCs.

These results strongly suggest that Liv8-positive cells include both immature and mature hematopoietic cells.

Liv8-negative BMCs significantly reduced liver fibrosis compared with that of the liver treated with CCl4 alone for 8 weeks, although Liv8-positive BMCs had no effect on liver fibrosis (Table 2).

Microarray analysis of the liver 1 week after BMC transplantation indicated increased expression of MMP-2, MMP-9 and MMP-14 with decreased expression of tissue inhibitor of metalloproteinase-3 (TIMP-3) compared with that of the liver treated with CCl_4 alone for 5 weeks (Table 3). Because the expression of MMP-9 was marked, we investigated it in this model.

Immunohistochemistry of MMP-9 showed localization of these cells similar to that of transplanted BMCs (Fig. 5A). However, the liver treated with CCl_4 alone showed only a few MMP-9–positive nonparenchymal cells (black arrows, Fig. 5B).

The expression of MMP-9 with *in situ* hybridization coincided with the immunohistochemical staining of MMP-9 (Fig. 5C).

Table 1. Hydroxyproline Content

Treatment (No. of Mice)	Hydroxyproline (μg/g Liver)
CCl_4, 5 wk (8)	464 ± 93
CCl_4, 8 wk (8)	630 ± 93
CCl_4/BMT, 5 wk (8)	494 ± 74
CCl_4/BMT, 8 wk (8)	392 ± 59*†

NOTE. Mice were treated with CCl_4 for 4 weeks; then, 1 week or 4 weeks after bone marrow cell transplantation (BMT) or saline injection with CCl_4 treatment, they were killed to measure liver hydroxyproline content. Results are typical of 1 of 3 independent experiments.

*$P < .01$ vs. CCl_4 (8 weeks).

†$P < .05$ vs. CCl_4/BMT (5 weeks).

Although double fluorescent-positive cells were not seen in the liver treated with CCl_4 alone (Fig. 6A), double-positive yellow-colored cells (black arrows) were seen in the BMC-transplanted liver (Fig. 6B). With high magnification, double fluorescent immunohistochemistry showed the expression of MMP-9 (red) on the GFP-positive (green) cell surface (Fig. 6C).

A double fluorescent (anti-GFP with green color and anti–α-smooth muscle actin with red color) study indicated that a fine network pattern of stellate cells (red) existed in the liver treated with CCl_4 alone for 5 weeks (Fig. 7A). Conversely, GFP-positive green-colored cells (green arrow) were seen with a reduced fine network pattern (red arrow) in the liver 1 week after BMC transplantation (Fig. 7B). Double fluorescent-positive yellow-colored cells (yellow arrow), presumably stellate cells, were then seen without the fine network pattern (red arrow) in the liver 2 weeks after BMC transplantation (Fig. 7C). The shape of these cells was different from other GFP-positive cells, and the number of the double-positive cells was very small.

Next, we examined the direct activity of MMP-9 using *in situ* zymography. Film *in situ* zymographic analysis revealed strong gelatinolytic activity in the periportal area

Table 2. Hydroxyproline Content

Treatment (No. of mice)	Hydroxyproline (μg/g Liver)
CCl_4 (8)	687 ± 102
CCl_4/Liv8-positive (8)	638 ± 94
CCl_4/Liv8-negative (8)	415 ± 77*

NOTE. Mice were treated with CCl_4 for 4 weeks followed by transplantation with Liv8-positive or Liv8-negative BMCs or saline. After 4 weeks of CCl_4 treatment (total 8 weeks), mice were killed to measure liver hydroxyproline content. Results are typical of 1 of 3 independent experiments.

*$P < .01$ vs. CCl_4.

Table 3. Microarray Analysis

	CCl_4 + BMC vs. CCl_4 Alone	
	Increased	Decreased
MMP-2	1.7	
MMP-9	3.9	
MMP-14	2.1	
TIMP-3		0.67

NOTE. Mice were treated with CCl_4 for 4 weeks and were killed 1 week after BMC transplantation. Microarray analysis was performed using 3 livers from each group. The expression ratios (CCl_4 + BMC vs. CCl_4 alone) larger than 1.5 are shown. Values indicated are the difference between the mean values of 3 mice. Results are typical of 1 of 2 independent experiments.

coinciding with the location of MMP-9–positive BMCs compared with the liver treated with CCl_4 alone (Fig. 8).

This gelatinolytic activity was completely blocked by the addition of 1,10-phenanthroline, an MMP inhibitor (data not shown).

Finally, the mice that underwent BMC transplantation with continuous CCl_4 injection showed a gradually increased serum albumin level (Supplementary Fig. 3) resulting in a significantly improved survival rate after BMC transplantation compared with mice treated with CCl_4 alone (Supplementary Fig. 4).

Discussion

In this report, transplanted BMCs can degrade collagen fibers and clearly reduce liver fibrosis with strong expression of MMPs, especially MMP-9, as indicated by both *in situ* zymography and the double staining of GFP and MMP-9 using fluorescent microscopy. The reason for the strong expression of MMP-9 is still unknown.

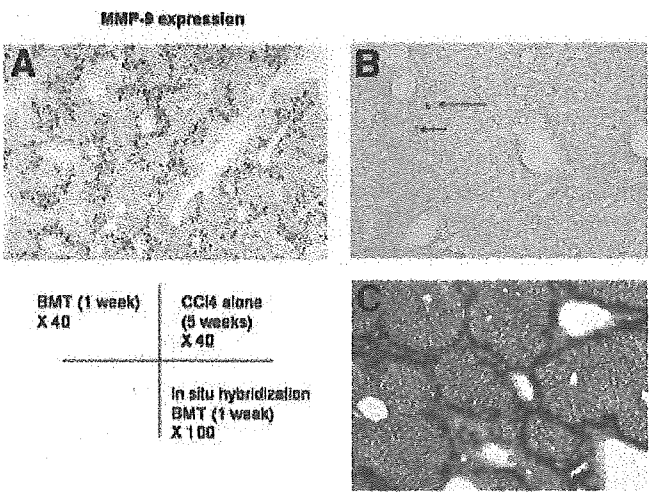

Fig. 5. Photomicrograph of a liver section stained with anti-MMP-9 antibody (A) from a mouse 1 week after BMC transplantation (BMT) and (B) from a mouse treated with CCl_4 alone for 5 weeks. (Original magnification, ×40.) (C) *In situ* hybridization of a liver section from a mouse 1 week after BMC transplantation. (Original magnification, ×100.)

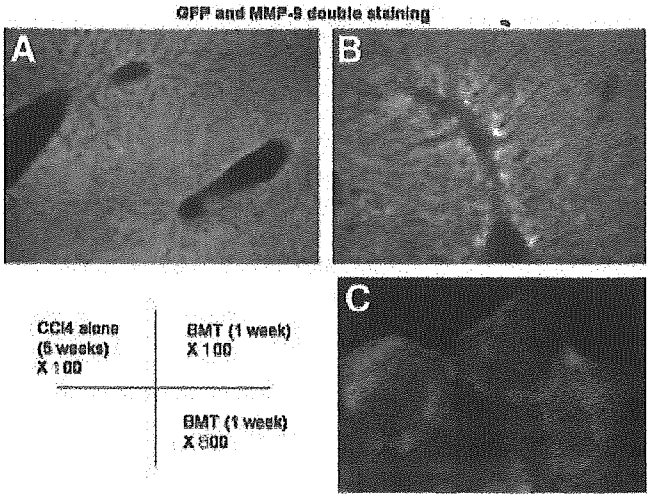

Fig. 6. Double fluorescent immunohistochemistry of a mouse liver after (A) 5-week treatment with CCl_4 alone and (B, C) 1 week after BMC transplantation (BMT) with CCl_4 treatment for 5 weeks. (Original magnification, [A and B] ×100; [C] ×800.)

However, Heissing et al.[20,21] recently reported that MMP-9 induced in BMCs released soluble Kit-ligand, which might be related to the transfer of stem cells in BMCs to the proliferative niche. Therefore, MMP-9 in our model could play an important role in the degradation of extracellular matrix and also by releasing some factors, *e.g.*, soluble Kit-ligand, related to the differentiation and proliferation of transplanted BMCs in liver inflammation induced by continuous injection of CCl_4. It has also been shown that MMP-9 plays an important role in the migration of mast progenitor cells to inflammatory

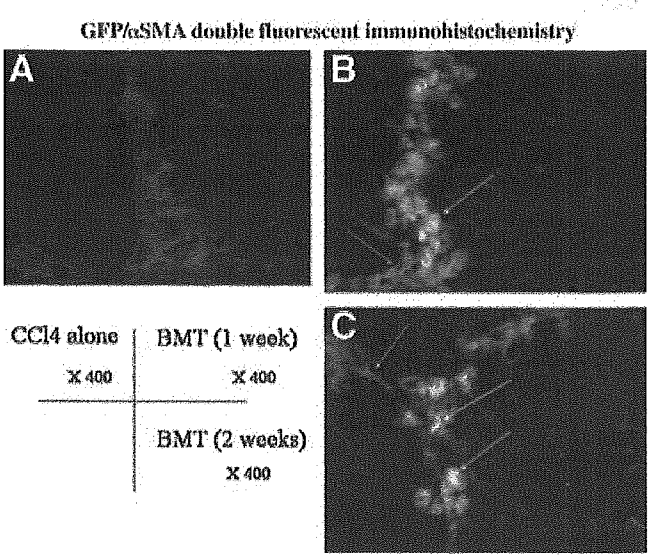

Fig. 7. Double fluorescent immunohistochemistry for α-smooth muscle actin (αSMA) and GFP of a mouse liver (A) treated with CCl_4 alone for 5 weeks and (B) 1 week, or (C) 2 weeks after BMC transplantation (BMT) with CCl_4 treatment. (Original magnification, ×400.)

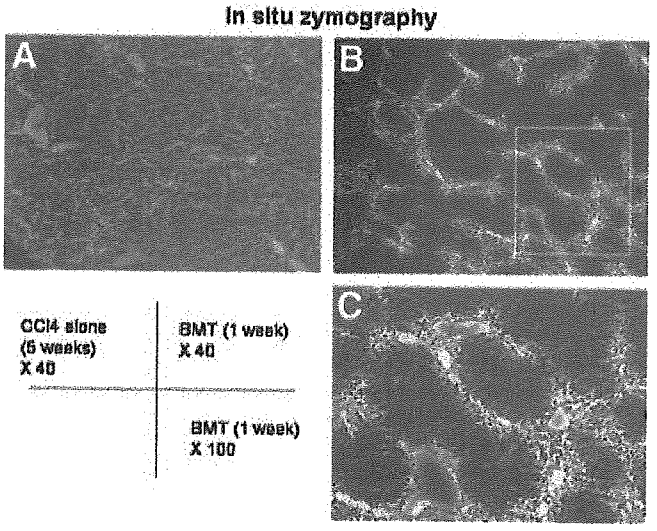

Fig. 8. *In situ* zymography of a mouse liver after (A) 5-week treatment with CCl_4 alone and (B, C) 1 week after BMC transplantation (BMT) with CCl_4 treatment for 5 weeks. (Original magnification, [A] ×40; [B] ×40, [C] ×100.)

tissue.[22,23] Therefore, the increased expression of MMP-9 in this study was somehow related to the migration of BMCs to the inflammatory liver.

Film *in situ* zymography clearly showed that these MMP-9–positive cells possessed high gelatinolytic activity compared with the liver treated with CCl_4 alone. Thus, the BMCs that migrated acted in the degradation of liver fibrosis (fibrolysis).

According to our present data, increased expression of MMP-14 (MT1-MMP [membrane-type 1 matrix metalloproteinase]) will contribute to degrading interstitial collagens[24] to gelatin that MMP-9 can degrade, resulting in the regression of fibrosis (fibrolysis).

Recently, Kollet et al.[25] reported that the expression of MMP-9 was increased with the migration of human $CD34^+$ progenitor cells in CCl_4-treated NOD/SCID mice and that an inhibitor of MMP-9 reduced this migration. Thus, proteolytic activity seems to be necessary for the cell migration in addition to matrix degradation activity.

It seems to be very important how many cells can migrate into the damaged liver to degrade fibers, but a recent paper[26] reported little evidence of bone marrow-derived hepatocytes in the CCl_4-treated liver. However, the dose of CCl_4 was only 4% (0.08 mL/kg) of our dose (0.5 mL/kg), and the number of mice used was too small (1 or 2). The reason they did not see the BMCs that migrated is most likely due to the cessation of CCl_4 injection after BMC transplantation. Even in our experimental model,[11] the cessation of CCl_4 after BMC transplantation dramatically reduced the number of BMCs migrating into the damaged liver (I.S., unpublished data, 2003). Thus, the extent of continuing liver damage may limit BMC migration to the liver with matrix degradation activity.

Transplanted BMCs differentiated into albumin-producing hepatocytes with an increased serum albumin level, and the degradation of the extracellular matrix may presumably lead to improved liver function resulting in better survival of mice with BMCtransplantation compared to that of treated with CCl_4 alone, although only 1 transplantation of BMCs was performed.

As shown by double fluorescence, our data may also indicate that transplanted BMCs seem to become stellate cells, in agreement with a recent report,[27] although the number was very small in our experimental model. This result seems to be contradictory to our result of resolution of liver fibrosis by BMC transplantation because transdifferentiated stellate cells may produce collagens. Our preliminary results indicated reduced messenger RNA expression of type I procollagen, transforming growth factor-β1 (TGF-β1) and no change of hepatocyte growth factor messenger RNA expression in the liver 1 week after BMC transplantation compared with the liver treated with CCl_4 alone (I. Sakaida, unpublished data, 2003). As shown in Fig. 7, migrated BMCs seemed to reduce the fine network pattern of activated stellate cells. Thus, transplanted BMCs may affect activated stellate cells by reducing their number—*e.g.*, by leading them to apoptosis. However, further examinations are necessary to determine the exact relationship between BMCs and resident stellate cells.

Our recent data[12] indicated that the subpopulation of BMCs, nonhematopoietic cells in bone marrow, separated using an anti-Liv8 antibody, will transdifferentiate into hepatocytes in the liver damaged by CCl_4 induction. The present study clearly indicates that this subpopulation of BMCs is also responsible for the resolution of liver fibrosis (fibrolysis) induced by CCl_4 treatment.

In conclusion, the present study introduces a new concept for the treatment of liver fibrosis.

References

1. Petersen BE, Bowen WC, Patrene KD, Mars WM, Sullivan AK, Murase N, et al. Bone marrow as a potential source of hepatic oval cells. Science 1999;284:1168–1170.
2. Theise ND, Nimmakayalu M, Gardner R, Illei PB, Morgan G, Teperman L, et al. Liver from bone marrow in humans. HEPATOLOGY 2000;32:11–16.
3. Alison MR, Poulsom R, Jeffery R, Dhillon AP, Quaglia A, Jacob J, et al. Hepatocytes from nonhepatic adult stem cells. Nature 2000;406:257.
4. Krause DS, Theise ND, Collector MI, Henegariu O, Hwang S, Gardner R, et al. Multi-organ, multi-lineage engraftment by a single bone marrow-derived stem cell. Cell 2001;105:369–377.
5. Lagasse E, Connors H, Al-Dhalimy M, Reitsma M, Dohse M, Osborne L, et al. Purified hematopoietic stem cells can differentiate into hepatocytes in vivo. Nat Med 2000;6:1229–1234.

6. Orlic D, Kajstura J, Chimenti S, Jakoniuk I, Anderson SM, Li B, et al. Bone marrow cells regenerate infarcted myocardium. Nature 2001;410: 701–705.
7. Korbling M, Katz RL, Khanna A, Ruifrok AC, Rondon G, Albitar M, et al. Hepatocytes and epithelial cells of donor origin in recipients of peripheral-blood stem cells. N Engl J Med 2002;346:738–746.
8. Okamoto R, Yajima T, Yamazaki M, Kanai T, Mukai M, Okamoto S, et al. Damaged epithelia regenerated by bone marrow-derived cells in the human gastrointestinal tract. Nat Med 2002;8:1011–1017.
9. Wagers AJ, Sherwood RI, Christensen JL, Weissman IL. Little evidence for developmental plasticity of adult hematopoietic stem cells. Science 2002; 297:2256–2259.
10. Okabe M, Ikawa M, Kominami K, Nakanishi T, Nishimune Y. "Green mice" as a source of ubiquitous green cells. FEBS Lett 1997;407:313–319.
11. Terai S, Sakaida I, Yamamoto N, Omori K, Watanabe T, Ohata S, et al. An in vivo model for monitoring trans-differentiation of bone marrow cells into functional hepatocytes. J Biochem (Tokyo). 2003;134:551–558.
12. Yamamoto N, Terai S, Ohata S, Watanabe T, Omori K, Shinoda K, et al. A subpopulation of bone marrow cells depleted by a novel antibody, anti-Liv8, is useful for cell therapy to repair damaged liver. Biochem Biophys Res Commun 2004;313:1110–1118.
13. Watanabe T, Nakagawa K, Ohata S, Kitagawa D, Nishitai G, Seo J, et al. SEK1/MKK4-mediated SAPK/JNK signaling participates in embryonic hepatoblast proliferation via a pathway different from NF-kappaB-induced anti-apoptosis. Dev Biol 2002;250:332–347.
14. Sakaida I, Uchida K, Matsumura Y, Okita K. Interferon gamma treatment prevents procollagen gene expression without affecting transforming growth factor-beta1 expression in pig serum-induced rat liver fibrosis in vivo. J Hepatol 1998;28:471–479.
15. Sakaida I, Nagatomi A, Hironaka K, Uchida K, Okita K. Quantitative analysis of liver fibrosis and stellate cell changes in patients with chronic hepatitis C after interferon therapy. Am J Gastroenterol 1999;94:489–496.
16. Sakaida I, Tsuchiya M, Kawaguchi K, Kimura T, Terai S, Okita K. Herbal medicine Inchin-ko-to (TJ-135) prevents liver fibrosis and enzyme-altered lesions in rat liver cirrhosis induced by a choline-deficient L-amino acid-defined diet. J Hepatol 2003;38:762–769.
17. Sakaida I, Hironaka K, Uchida K, Suzuki C, Kayano K, Okita K. Fibrosis accelerates the development of enzyme-altered lesions in the rat liver. HEPATOLOGY 1998;28:1247–1252.
18. Jimenez MJ, Balbin M, Lopez JM, Alvarez J, Komori T, Lopez-Otin C. Collagenase 3 is a target of Cbfa1, a transcription factor of the runt gene family involved in bone formation. Mol Cell Biol 1999;19:4431–4442.
19. Nakada M, Nakamura H, Ikeda E, Fujimoto N, Yamashita J, Sato H, et al. Expression and tissue localization of membrane-type 1, 2, and 3 matrix metalloproteinases in human astrocytic tumors. Am J Pathol 1999;154: 417–428.
20. Heissig B, Hattori K, Dias S, Friedrich M, Ferris B, Hackett NR, et al. Recruitment of stem and progenitor cells from the bone marrow niche requires MMP-9 mediated release of kit-ligand. Cell 2002;109:625–637.
21. Hattori K, Heissig B, Wu Y, Dias S, Tejada R, Ferris B, et al. Placental growth factor reconstitutes hematopoiesis by recruiting VEGFR1(+) stem cells from bone-marrow microenvironment. Nat Med 2003;8:841–849.
22. Tanaka A, Arai K, Kitamura Y, Matsuda H. Matrix metalloproteinase-9 production, a newly identified function of mast cell progenitors, is down-regulated by c-kit receptor activation. Blood 1999;94:2390–2395.
23. Baram D, Vaday GG, Salamon P, Drucker I, Hershkoviz R, Mekori YA. Human mast cells release metalloproteinase-9 on contact with activated T cells: juxtacrine regulation by TNF-alpha. J Immunol 2001;167:4008–4016.
24. Ohuchi E, Imai K, Fujii Y, Sato H, Seiki M, Okada Y. Membrane type 1 matrix metalloproteinase digests interstitial collagens and other extracellular matrix macromolecules. J Biol Chem 1997;272:2446–2451.
25. Kollet O, Shivtiel S, Chen YQ, Suriawinta J, Thung SN, Dabeva MD, et al. HGF, SDF-1, and MMP-9 are involved in stress-induced human CD34+ stem cell recruitment to the liver. J Clin Invest 2003;112:160–169.
26. Kanazawa Y, Verma IM. Little evidence of bone marrow-derived hepatocytes in the replacement of injured liver. Proc Natl Acad Sci U S A 2003; 100(Suppl);11850–11853.
27. Forbes SJ, Russo FP, Rey V, Burra P, Rugge M, Wright NA, et al. A significant proportion of myofibroblasts are of bone marrow origin in human liver fibrosis. Gastroenterology 2004;126:955–963.

Available online at www.sciencedirect.com
SCIENCE DIRECT®
Toxicology Letters 152 (2004) 175–181
Toxicology Letters
www.elsevier.com/locate/toxlet

Requirement of MKK4 and MKK7 for $CdCl_2$- or $HgCl_2$-induced activation of c-Jun NH_2-terminal kinase in mouse embryonic stem cells

Masato Matsuoka [a,b,*], Hideki Igisu [b], Kentaro Nakagawa [c], Toshiaki Katada [c], Hiroshi Nishina [c]

[a] *Department of Hygiene and Public Health (1), School of Medicine, Tokyo Women's Medical University, 8-1 Kawada-cho, Shinjuku-ku, Tokyo 162-8666, Japan*
[b] *Department of Environmental Toxicology, Institute of Industrial Ecological Sciences, University of Occupational and Environmental Health, 1-1 Iseigaoka, Yahatanishi-ku, Kitakyushu 807-8555, Japan*
[c] *Department of Physiological Chemistry, Graduate School of Pharmaceutical Sciences, University of Tokyo, 7-3-1 Hongo, Bunkyo-ku, Tokyo 113-0033, Japan*

Received 10 March 2004; received in revised form 27 April 2004; accepted 28 April 2004

Available online 15 June 2004

Abstract

c-Jun NH_2-terminal kinase (JNK), also known as stress-activated protein kinase (SAPK), is activated primarily by inflammatory cytokines and environmental stresses including toxic metal exposure. To reveal the upstream kinase responsible for JNK activation by toxic metals, the phosphorylation status and the activity of JNK were examined in mouse embryonic stem (ES) cells lacking MKK4 or MKK7 following exposure to $CdCl_2$ or $HgCl_2$. Treatment with $CdCl_2$ or $HgCl_2$ induced the phosphorylation of JNK in a dose- and time-dependent manner in wild-type ES cells. In both *mkk4*$^{-/-}$ and *mkk7*$^{-/-}$ ES cells, $CdCl_2$- or $HgCl_2$-induced phosphorylation and activation of JNK were suppressed significantly. However, in *mkk7*$^{-/-}$ ES cells treated with $CdCl_2$ and $HgCl_2$, JNK activation was not abolished (suppressed by 56% and 78%, respectively). These findings suggest that the full activation of JNK by toxic metal exposure requires both MKK4 and MKK7, and these upstream kinases might contribute differentially in JNK activation between mouse ES cells exposed to $CdCl_2$ and $HgCl_2$.

Keywords: c-Jun NH_2-terminal kinase; MKK4; MKK7; $CdCl_2$; $HgCl_2$; ES cells

1. Introduction

Mitogen-activated protein kinases (MAPKs) are a family of Ser/Thr protein kinases that transmit signals into the nucleus, and have been shown to participate in a diverse array of cellular functions such as the control of gene expression, cell proliferation, differentiation, development, inflammatory response, and

Abbreviations: JNK, c-Jun NH_2-terminal kinase; SAPK, stress-activated protein kinase; ES, embryonic stem; MAPK, mitogen-activated protein kinase; ERK, extracellular signal-regulated protein kinase

* Corresponding author. Tel.: +81-3-3353-8111; fax: +81-3-5269-7419.
E-mail address: matsuoka@research.twmu.ac.jp (M. Matsuoka).

0378-4274/$ – see front matter © 2004 Elsevier Ireland Ltd. All rights reserved.
doi:10.1016/j.toxlet.2004.04.033

apoptosis in mammalian systems (Chang and Karin, 2001; Weston and Davis, 2002). c-Jun NH_2-terminal kinase (JNK), also known as stress-activated protein kinase (SAPK), represents one subgroup of MAPKs that is activated primarily by inflammatory cytokines and environmental stresses such as ultraviolet radiation, ionizing radiation, heat shock, osmotic shock, protein synthesis inhibitor, and chemical mutagens (Kyriakis and Avruch, 1996; Robinson and Cobb, 1997). In addition, we have found that environmentally contaminating toxic metals such as cadmium (Matsuoka and Igisu, 1998), inorganic mercury (Matsuoka et al., 2000), and tributyltin (Yu et al., 2000) activate JNK pathway. However, functions and molecular mechanisms of toxic metal-induced JNK activation have not yet been known.

For the activation, JNK requires the dual phosphorylation of Thr and Tyr residues located in a Thr-Pro-Tyr motif between kinase subdomains VII and VIII (Cobb and Goldsmith, 1995). This phosphorylation is catalyzed by the dual specific kinases MKK4 (also known as SEK1 or MEK4) and MKK7 (SEK2), while MKK4 has a preference for the Tyr residue and MKK7 for the Thr residue (Weston and Davis, 2002). In vitro, JNK is activated synergistically by these two upstream kinases (Lawler et al., 1998). With respect to cadmium, it has been reported that JNK activation was suppressed partially by expression of dominant negative mutant of MKK7, but not that of MKK4 in human non-small-cell lung carcinoma cells (Chuang and Yang, 2001; Chuang et al., 2000) and rat mesangial cells (Ding and Templeton, 2000). These findings suggest that cadmium might activate JNK through MKK7, but not MKK4 in vivo. On the other hand, the activation of JNK by ultraviolet, heat shock, sorbitol-induced osmolarity change, or the protein synthesis inhibitor anisomycin was markedly attenuated in mouse embryonic stem (ES) cells targeting either the *mkk4* or the *mkk7* gene (Kishimoto et al., 2003), indicating that both MKK4 and MKK7 are required for the activation of JNK by these stimuli in mouse ES cells. To clarify whether signaling pathway leading to JNK activation by toxic metals is distinct from the case of other cellular stresses, the phosphorylation status and the activity of JNK were examined in $mkk4^{-/-}$ and $mkk7^{-/-}$ ES cells following exposure to $CdCl_2$ or $HgCl_2$. The application of these ES cells lacking either MKK4 or MKK7 would be more beneficial than other cells expressed with dominant negative form of them.

2. Materials and methods

2.1. Cell culture and treatments

The murine ES cell line E14K (wild-type), $mkk4^{-/-}$ mutant cell line made by the *mkk4* gene targeting (Nishina et al., 1997), and $mkk7^{-/-}$ mutant cell line made by the *mkk7* gene targeting (Kishimoto et al., 2003) were maintained in Dulbecco's modified Eagle's medium supplemented with 15% fetal calf serum (GIBCO, Invitrogen Corp., Carlsband, CA, USA) and leukemia inhibitory factor as described previously (Kishimoto et al., 2003). Wild-type, $mkk4^{-/-}$ and $mkk7^{-/-}$ ES cells (passage number 10–15) were plated at 5×10^5 cells per well (for Western immunoblotting) or 1.6×10^6 cells per well (for JNK activity assay) in six-well culture plates coated with 1% gelatin, and cultured for overnight. Then, medium was changed to serum-free medium containing $CdCl_2$ (Sigma Chemical Co., St. Louis, MO, USA) or $HgCl_2$ (Nacalai Tesque, Osaka, Japan). Untreated control cells were incubated with serum-free medium, and were treated identically to cells incubated with $CdCl_2$ or $HgCl_2$. Initially, dose (1 μM, 5 μM, 10 μM, 20 μM, or 40 μM) and time (5 min, 15 min, 30 min, 45 min, or 60 min) of $CdCl_2$ or $HgCl_2$ exposure for the sufficient induction of JNK phosphorylation were determined in wild-type ES cells. Based on these experiments, each ES cell line was incubated with 20 μM of $CdCl_2$ or $HgCl_2$ for 1 h. All experiments were repeated three (for Western immunoblotting) or four times (for JNK activity assay). Data were all obtained from two independently derived ES cell clones with comparable results.

2.2. Western immunoblotting

After the incubation with $CdCl_2$ or $HgCl_2$, ES cells were washed with phosphate-buffered saline, and lysed with sodium dodecyl sulfate (SDS)-polyacrylamide gel Laemmli sample buffer. Cell lysates were collected, sonicated, and boiled for 5 min. Twenty micrograms of protein was subjected to SDS-polyacrylamide gel electrophoresis on a 10%

polyacrylamide gel and transferred to a nitrocellulose membrane (Hybond-ECL, Amersham Pharmacia Biotech, Buckinghamshire, England). The membrane was blocked with 5% non-fat milk or bovine serum albumin in Tris-buffered saline containing 0.1% Tween 20 for 1 h at room temperature. The membrane was incubated overnight at 4 °C with the primary antibody diluted 1:1000. The antibodies used were phospho-SAPK/JNK (Thr^{183}/Tyr^{185}) antibody, phosphorylation state-independent SAPK/JNK antibody, phospho-p38 MAPK (Thr^{180}/Tyr^{182}) antibody, phosphorylation state-independent p38 MAPK antibody, phospho-p44/42 MAPK (Thr^{202}/Tyr^{204}) antibody, phosphorylation state-independent p44/42 MAPK antibody, phospho-specific c-Jun (Ser^{63}) antibody (Cell Signaling Technology, Inc., Beverly, MA, USA), anti-ACTIVE JNK antibody (Promega Corporation, Madison, IL, USA), MEK-4 (C-20) antibody (Santa Cruz Biotechnology Inc., Santa Cruz, CA, USA), and rat monoclonal antibody against MKK7 (KN-004) prepared by Kishimoto et al. (2003). Protein was detected with a Phototope-HRP Western blot detection kit (Cell Signaling Technology). For the detection of MKK7 protein, a SuperSignal West Femto Maximum Sensitivity Substrate (Pierce Chemical Co., Rockford, IL, USA) was used. After the immunodetection, some blots were incubated with a Restore Western Blot Stripping Buffer (Pierce) for 30 min at room temperature, and reprobed with each phosphorylation state-independent MAPK antibody. The bands on the developed films were quantified with NIH Image Version 1.63.

2.3. JNK activity assay

The in vitro activity of JNK was measured using a SAPK/JNK assay kit (Cell Signaling Technology) according to the instruction from the manufacturer. Briefly, cell lysates were incubated with GST-c-Jun (1–89) fusion protein overnight, and the precipitated JNK was subjected to in vitro kinase assay using GST-c-Jun (1–89) as substrate. Phosphorylation of GST-c-Jun on Ser^{63} was analyzed with immunoblotting using phospho-c-Jun antibody. The bands on the developed films were quantified with NIH Image Version 1.63.

2.4. Statistical analysis

Results were expressed as mean ± S.D. The statistical significance was determined by one-way analysis of variance followed by the Dunnett multiple comparison test. $P < 0.05$ was considered as statistically significant.

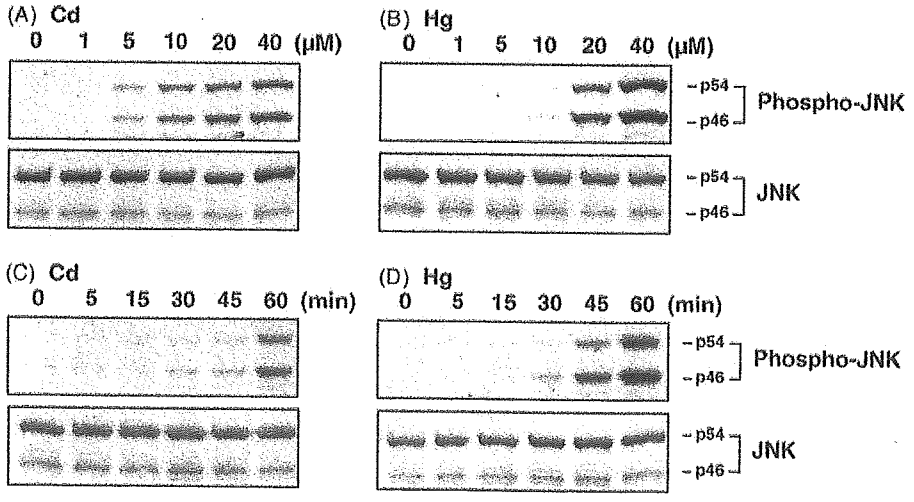

Fig. 1. Dose effects (A, B) and time course (C, D) of $CdCl_2$- or $HgCl_2$-induced accumulation of phosphorylated JNK in wild-type ES cells. Wild-type ES cells were incubated with 0 μM, 1 μM, 5 μM, 10 μM, 20 μM, or 40 μM $CdCl_2$ (A) or $HgCl_2$ (B) for 1 h. In the time course study, cells were incubated with 20 μM $CdCl_2$ (C) or $HgCl_2$ (D) for 5–60 min. The untreated control is 0 min. Cell lysates were subjected to immunoblotting using anti-phospho-JNK and anti-JNK antibodies. Results shown are representative of three independent experiments.

3. Results

3.1. $CdCl_2$- or $HgCl_2$-induced accumulation of phosphorylated JNK in wild-type ES cells

When wild-type ES cells were incubated with 5 μM of $CdCl_2$ or 20 μM of $HgCl_2$ for 1 h, phosphorylation of JNK (p46 and p54) was found, and the levels of phosphorylated form of JNK increased in a concentration-dependent manner (Fig. 1A and B). In contrast, the levels of total (phosphorylation state-independent) JNK were not changed by incubation with any concentration of $CdCl_2$ or $HgCl_2$. In the time course study, the levels of phosphorylated JNK increased after 30 min or 45 min in response to 20 μM $CdCl_2$ or $HgCl_2$ exposure, whereas total JNK levels were not changed (Fig. 1C and D). Thereafter, ES cells were exposed to $CdCl_2$ or $HgCl_2$ for 1 h at a concentration of 20 μM.

3.2. Suppression of $CdCl_2$- or $HgCl_2$-induced JNK activation in $mkk4^{-/-}$ and $mkk7^{-/-}$ ES cells

As shown in Fig. 2, MKK4 and MKK7 proteins were not detected in $mkk4^{-/-}$ and $mkk7^{-/-}$ ES cells, respectively. Neither MKK4 expression in wild-type and $mkk7^{-/-}$ ES cells nor MKK7 expression in wild-type and $mkk4^{-/-}$ ES cells was affected by the treatment with $CdCl_2$ or $HgCl_2$. In $mkk4^{-/-}$ ES cells, $CdCl_2$- or $HgCl_2$-induced phosphorylation of JNK was abolished almost completely without changing JNK levels (Fig. 3A, lanes 5 and 6). While toxic

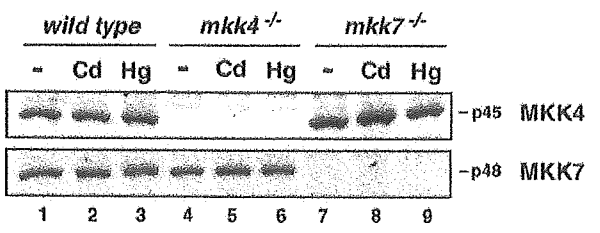

Fig. 2. Effects of $CdCl_2$ or $HgCl_2$ treatment on the levels of MKK4 and MKK7 in wild-type, $mkk4^{-/-}$ and $mkk7^{-/-}$ ES cells. Wild-type, $mkk4^{-/-}$ and $mkk7^{-/-}$ ES cells were incubated with serum-free medium (lanes 1, 4, and 7), 20 μM $CdCl_2$ (lanes 2, 5, and 8) or 20 μM $HgCl_2$ (lanes 3, 6, and 9) for 1 h, and cell lysates were subjected to immunoblotting using anti-MKK4 and anti-MKK7 antibodies. Results shown are representative immunoblot of three independent experiments.

metal-induced JNK phosphorylation in $mkk7^{-/-}$ ES cells was also reduced significantly, JNK phosphorylation in $mkk7^{-/-}$ ES cells treated with $CdCl_2$ and $HgCl_2$ was 55% and 33% of that in wild-type ES cells treated, respectively (Fig. 3A, lanes 8 and 9). These findings were reproducible with two different anti-phospho-JNK antibodies used in the present study. In contrast to JNK, substantial phosphorylation of other members of MAPK family, p38 and extracellular signal-regulated protein kinase (ERK2/p42 and ERK1/p44), were observed in both, $mkk4^{-/-}$ and $mkk7^{-/-}$ ES cells treated with $CdCl_2$ or $HgCl_2$ (Fig. 3B and C, lanes 5, 6, 8 and 9).

The in vitro activity of JNK assayed using GST-c-Jun as substrate was also examined. Treatment with $CdCl_2$ or $HgCl_2$ induced the marked elevation of JNK activity in wild-type ES cells (Fig. 4, lanes 2 and 3). Consistent with the reduction of phosphorylated JNK levels (Fig. 3A), $CdCl_2$- or $HgCl_2$-induced JNK activation was suppressed in both $mkk4^{-/-}$ and $mkk7^{-/-}$ ES cells. JNK activity in $mkk4^{-/-}$ ES cells treated with $CdCl_2$ and $HgCl_2$ was 12% and 11% of that in wild-type ES cells treated, respectively (Fig. 4, lanes 5 and 6). JNK activity in $mkk7^{-/-}$ ES cells treated with $CdCl_2$ and $HgCl_2$ was 44% and 22% of that in wild-type ES cells treated, respectively (Fig. 4, lanes 8 and 9). Determination of JNK activity based on $[\gamma - {}^{32}P]$ incorporation into GST-c-Jun also showed the significant reduction of $CdCl_2$-induced JNK activation in both, $mkk4^{-/-}$ and $mkk7^{-/-}$ ES cells (Nakagawa et al., unpublished data).

4. Discussion

The present study showed that treatment with $CdCl_2$ or $HgCl_2$ induced the accumulation of phosphorylated form of JNK in a dose- and time-dependent manner in wild-type ES cells as has been observed in the various cell types (Matsuoka and Igisu, 2002). In both, $mkk4^{-/-}$ and $mkk7^{-/-}$ ES cells which lack an upstream JNK activator, $CdCl_2$- or $HgCl_2$-induced phosphorylation and activation of JNK were suppressed dramatically. However, in $mkk7^{-/-}$ ES cells treated with $CdCl_2$ and $HgCl_2$, JNK activation was not abolished (suppressed by 56% and 78%, respectively). On the other hand, significant phosphorylation of other members of MAPK, p38 and ERK, was retained in

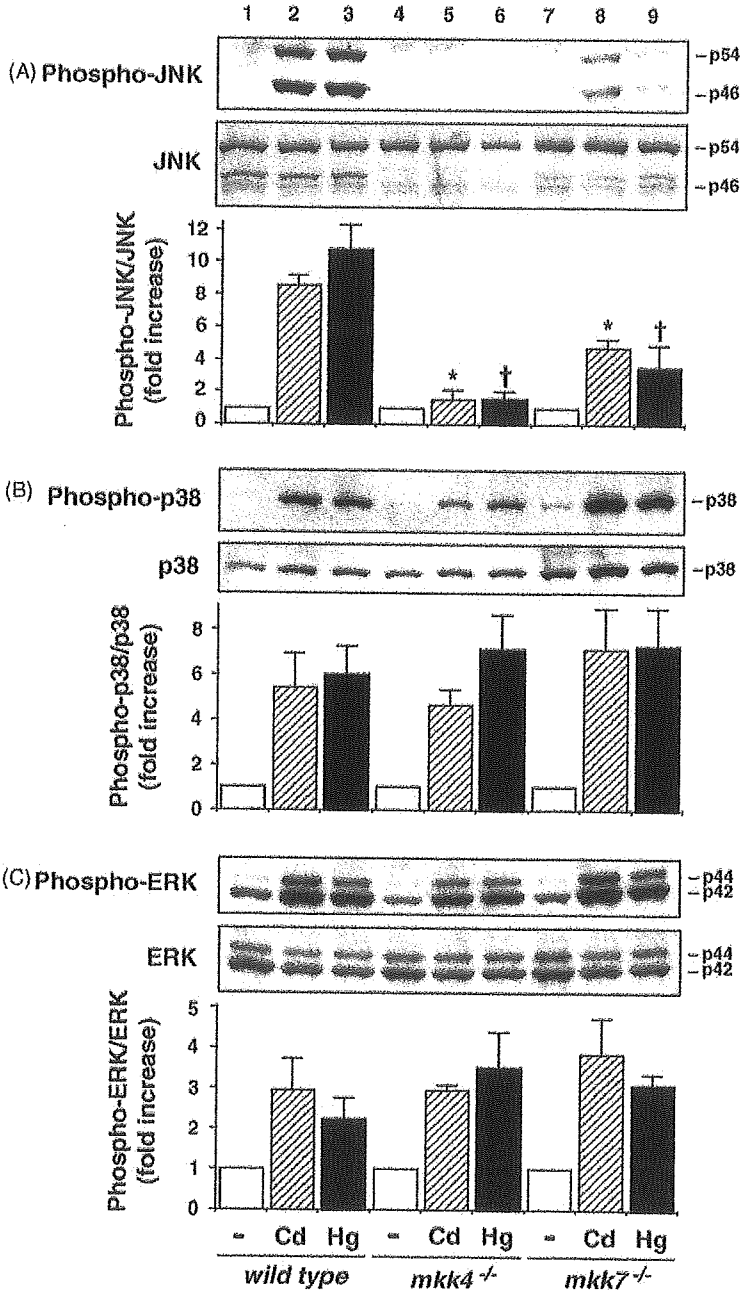

Fig. 3. Effects of $CdCl_2$ or $HgCl_2$ treatment on the levels of phosphorylated JNK (A), phosphorylated p38 (B), and phosphorylated ERK (C). Wild-type, *mkk4*$^{-/-}$ and *mkk7*$^{-/-}$ ES cells were incubated with serum-free medium (lanes 1, 4, and 7), 20 μM $CdCl_2$ (lanes 2, 5, and 8) or 20 μM $HgCl_2$ (lanes 3, 6, and 9) for 1 h, and cell lysates were subjected to immunoblotting using anti-phospho-JNK and anti-JNK antibodies (A), anti-phospho-p38 and anti-p38 antibodies (B), and anti-phospho-ERK and anti-ERK antibodies (C). Results shown are representative immunoblot and densitometric analysis of phosphorylated JNK, p38 and ERK. Each value was expressed as the ratio of phosphorylated MAPK level to the corresponding total MAPK level, and the value of control (without metal treatments) was set to one. Each column and bar represent the mean ± S.D. of three independent experiments. $^{*}P < 0.01$ compared to wild-type ES cells treated with $CdCl_2$, $^{\dagger}P < 0.01$ compared to wild-type ES cells treated with $HgCl_2$.